



This is the accepted manuscript made available via CHORUS. The article has been published as:

Final-state interactions and spin structure in  ${}^1\text{Li}$  breakup of  ${}^{11}\text{Li}$  in halo effective field theory

Matthias Göbel, Bijaya Acharya, Hans-Werner Hammer, and Daniel R. Phillips

Phys. Rev. C **107**, 014617 — Published 25 January 2023

DOI: [10.1103/PhysRevC.107.014617](https://doi.org/10.1103/PhysRevC.107.014617)

# Final-state interactions and spin structure in $E1$ breakup of $^{11}\text{Li}$ in Halo Effective Field Theory

Matthias Göbel,<sup>1,\*</sup> Bijaya Acharya,<sup>2,3</sup> Hans-Werner Hammer,<sup>1,4</sup> and Daniel R. Phillips<sup>3</sup>

<sup>1</sup>*Technische Universität Darmstadt, Department of Physics,  
Institut für Kernphysik, 64289 Darmstadt, Germany*

<sup>2</sup>*Physics Division, Oak Ridge National Laboratory, Oak Ridge, TN 37831, USA*

<sup>3</sup>*Institute of Nuclear and Particle Physics and Department of Physics and Astronomy, Ohio University, Athens, OH 45701, USA*

<sup>4</sup>*ExtreMe Matter Institute EMMI and Helmholtz Forschungsakademie Hessen für FAIR (HFHF),  
GSI Helmholtzzentrum für Schwerionenforschung GmbH, 64291 Darmstadt, Germany*

(Dated: November 22, 2022)

We calculate the  $E1$  breakup of the  $2n$  halo nucleus  $^{11}\text{Li}$  in Halo Effective Field Theory (Halo EFT) at leading order. In Halo EFT,  $^{11}\text{Li}$  is treated as a three-body system of a  $^9\text{Li}$  core and two neutrons. We present a detailed investigation of final-state interactions (FSI) in the neutron-neutron ( $nn$ ) and neutron-core ( $nc$ ) channels. We employ Møller operators to formulate an expansion scheme that satisfies the non-energy-weighted cluster sum rule and successively includes higher-order terms in the multiple-scattering series for the FSI. Computing the  $E1$  strength up to third order in this scheme, we observe apparent convergence and good agreement with experiment. The neutron-neutron FSI is by far the most important contribution and largely determines the maximum value of the  $E1$  distribution. However, inclusion of  $nc$  FSI does shift the peak position to slightly lower energies. Moreover, we investigate the sensitivity of the  $E1$  response to the spin structure of the neutron- $^9\text{Li}$  interaction. We contrast results for an interaction that is the same in the spin-1 and spin-2 channels with one that is only operative in the spin-2 channel, and find that good agreement with experimental data is only obtained if the interaction is present in both spin channels. The latter case is shown to be equivalent to a calculation in which the spin of  $^9\text{Li}$  is neglected.

## I. INTRODUCTION

Halo nuclei consist of a compact core and one or more loosely bound valence nucleons. As a consequence, they are significantly larger than neighbouring nuclei in their isotopic chain. Neutron halos are the most universal halo systems as their halo structure is not altered by the long-range Coulomb interaction [1, 2]. They were discovered in the 1980's at radioactive beam facilities by measuring their unusually large interaction radius [3]. Jonson and Hansen subsequently showed that this large radius is connected to a small separation energy of the halo neutrons [4].

The corresponding separation of energy scales forms the basis for a controlled description of halo nuclei in the framework of Halo Effective Field Theory (Halo EFT) [2, 5, 6], which systematizes cluster models of halo nuclei. The breakdown scale  $M_{\text{core}}$  is the lowest momentum scale not explicitly included in the theory. This is set by the excitation energy of the core, or by the size of the core, whichever yields the smaller momentum scale. The EFT exploits that the momentum scale of the halo nucleons set by their separation energy is much smaller,  $M_{\text{halo}} \ll M_{\text{core}}$ . Typically  $M_{\text{halo}}$  is of order tens of MeV for halo nuclei, while, the breakdown momentum scale,  $M_{\text{core}}$ , varies between 50 and 150 MeV. The EFT expansion is then in powers of  $M_{\text{halo}}/M_{\text{core}}$ , and for a typical momentum of order  $M_{\text{halo}}$  the EFT uncertainty is of order  $(M_{\text{halo}}/M_{\text{core}})^{n+1}$  for a calculation at order  $n$ . Halo EFT describes the structural properties of one- and two-neutron halo nuclei with nucleon-nucleon and nucleon-core interactions. It has also been applied to a number of electromagnetic and weak observables, including capture reactions, photodissociation processes, and weak decays (see, e.g., Refs. [2, 7–10] for a review and some recent references.)

In this work, we focus on Coulomb dissociation which is a powerful tool to study the structure of halo nuclei. The electric dipole transition strength, which is enhanced at low excitation energies for halo nuclei, is probed in Coulomb dissociation experiments by accelerating them to high energies and scattering them peripherally off a high- $Z$  target. This “soft dipole mode” has been under intense investigation both in experiment and in theory since the discovery of halo nuclei in the early 80's [11]. Halo EFT was first applied to Coulomb dissociation of the one-neutron halo  $^{11}\text{Be}$  [12]. Further work extended the description to  $^{19}\text{C}$  [13]. In Ref. [2], it was shown that the  $E1$  excitation of one-neutron halo nuclei can be described by a dimensionless universal function of the energy in units of the one-neutron separation energy.

---

\* E-mail: goebel@theorie.ikp.physik.tu-darmstadt.de

The  $E1$  response of a two-neutron halo is also expected to be governed by a universal function [14], in close analogy to the one-neutron case discussed above. In this work, we discuss the  $E1$  response of  $^{11}\text{Li}$ . Lithium-11 was previously considered in Halo EFT in Refs. [15–18]. Both  $^{11}\text{Li}$  and the  $^9\text{Li}$  core have the quantum number  $J^P = 3/2^-$ , while the unbound  $^{10}\text{Li}$  appears to have a low-energy anti-bound state with quantum numbers  $J^P = 2^-$  or  $1^-$ .

The two-neutron separation energy of  $^{11}\text{Li}$  is 0.369 MeV and the  $^{10}\text{Li}$   $s$ -wave resonance<sup>1</sup> is 26(13) keV above the  $^9\text{Li}$ - $n$  threshold [19]. The momentum scale  $M_{\text{halo}}$  can be estimated from these energy scales using  $M \sim \sqrt{mE}$  as  $M_{\text{halo}} = 18.6$  MeV. The first excitation energy of the  $^9\text{Li}$  ground state is 2.69 MeV [20] and its one-neutron separation energy is 4.06 MeV [19], while the charge radius of  $^9\text{Li}$  is 2.25 fm [21], implying a scale  $M_{\text{core}}$  of 50–90 MeV. This yields an expansion parameter of, at worst,  $M_{\text{halo}}/M_{\text{core}} \sim 0.37$ .

A leading-order Halo EFT calculation of  $^{11}\text{Li}$  should therefore be able to describe Coulomb dissociation data with reasonable accuracy. This was indeed found to be the case in preliminary Halo EFT calculations of this process [22–24] that showed good agreement with the  $E1$  strength extracted from Coulomb dissociation data in Ref. [25] at transition energies within the domain of validity of Halo EFT. These studies, as well as earlier work within three-body models in Refs. [26–28] found that, in contrast to the case of Coulomb dissociation of an  $s$ -wave one-neutron halo [23], final-state interactions (FSIs) play a significant role in determining the neutron spectrum measured in Coulomb dissociation of  $^{11}\text{Li}$ . This was also observed for other  $2n$  halos such as  $^{22}\text{C}$ , see, e.g., Ref. [29].

In this work, our aim is threefold:

- Obtain a description of the experimental  $E1$  breakup data from Ref. [25] in Halo EFT with theoretical uncertainties.
- Explore in detail the role of the  $nn$  and  $^9\text{Li}$ - $n$  FSIs in this process, paying particular attention to the constraints from the non-energy-weighted cluster sum rule for  $E1$  breakup.
- Investigate the impact of the spin structure of the  $^9\text{Li}$ - $n$  interaction, which is non-trivial because the  $^9\text{Li}$  core has spin  $3/2$ , and derive the relationship of such a calculation to the frequent assumption of a spin-0 core.

Before plunging into the details of our calculation we provide the reader with a list of the three approximations we make, and the reasons why we see them as not damaging to our goals:

1. We perform a leading-order three-body Halo EFT calculation of  $^{11}\text{Li}$  that neglects interactions which are higher order in the EFT power counting. This power counting tells us what mechanisms would be included at the next order and also provides us with an uncertainty estimate based on the scale separation in this problem.
2. We include the different final-state interactions using combinations of Møller operators. Compared to a full (e.g. Faddeev) calculation of the interacting three-body continuum this is an approximation. Because we perform calculations with different numbers of Møller operators, and consider them acting in different sequences, we gain some insight into the convergence of the multiple-scattering series for this problem.
3. We truncate in the quantum numbers of the final state in such a way that only states with minor contributions are neglected. The associated uncertainties are investigated by comparing the results obtained with different truncations. Moreover, there is also some truncation in the initial-state wave function components, which is also quantified. Such truncations are generic in treatments of the quantum-mechanical few-body problem.

Quantitative assessment of each of these approximations is provided in the body of the paper, and this list is recapitulated, along with those uncertainties, in the conclusion.

The fact that this is a leading-order Halo EFT calculations means that we include only  $s$ -wave interactions in our leading-order calculation—as was also the case in previous leading-order Halo EFT calculations [15–18]. We are aware that this is a different strategy to the one typically taken in three-body cluster models, many of which predict significant  $p$ -wave components in the wave function [30]. There is also experimental evidence for a mixing of different-parity components [31]. However, the different models given in Ref. [32] showed that already a calculation with only  $s$ -wave  $^9\text{Li}$ - $n$  interactions can yield momentum distributions in agreement with experimental data at an acceptable level at low momenta. More recently, Casal and Moro achieved a reasonable description of the  $^9\text{Li}(d,p)^{10}\text{Li}$  reaction using  $1^-/2^-$   $s$ -wave virtual states and  $1^+/2^+$   $p$ -wave resonances around 500 keV [33]. There seems to be no conclusive evidence for a  $p$ -wave resonance in the  $^9\text{Li}$ - $n$  system significantly below 500 keV, despite many investigations of this system over the years [34–38]. We therefore follow the Halo EFT power counting, which stipulates that  $p$ -wave

---

<sup>1</sup> Due to the mentioned inconclusive state of the literature this resonance is in many cases also understood as a virtual state. Moreover, there is some discussion whether  $^{10}\text{Li}$  can be a low-energy  $s$ -wave resonance. In principle the effective nuclear  $^9\text{Li}$ - $n$  interaction could form a barrier. Thereby  $^{10}\text{Li}$  could be a true resonance.

resonances at energies  $\approx 500$  keV, i.e., corresponding to momenta of order  $M_{halo}$ , produce only a NLO effect in the E1 response, unless they are kinematically enhanced because the experimental energy is tuned to the resonance energy.

The paper is structured as follows. In Sec. II we derive the leading-order wave function of  $^{11}\text{Li}$  in Halo EFT. We write down the Faddeev equations for this system and define the  $s$ -wave interactions that govern its structure at leading order in Halo EFT. We also elucidate the differences in these equations that result because  $^9\text{Li}$  is a spin-3/2 core and not a spin-0 core and discuss the circumstances under which the more complex spin situation encountered in this problem reduces to the case of a spin-0 core. In Sec. III we present our calculations of the E1 matrix element of the  $^{11}\text{Li}$  ground state and the non-interacting  $nnc$  scattering state and show how to use Møller operators to incorporate  $nc$  and  $nn$  final-state interactions. Moreover, we discuss the influence of different-spin  $nc$  interaction channels. In Sec. IV we show how to develop approximations to the final-state scattering wave function that preserve the non-energy-weighted sum rule, before concluding in Sec. V.

## II. $^{11}\text{Li}$ IN HALO EFT

A convenient ingredient for describing  $^{11}\text{Li}$  and calculating observables is its wave function. In our Halo EFT description this is the wave function of a three-body system. The wave function is a concept commonly known from quantum mechanics, that can also appear in a nonrelativistic field theory through its relation to the vertex function that is the residue of the three-body scattering amplitude at the bound-state pole (see, e.g., the review [2]). Since the corresponding half-off-shell amplitude appears in many calculations the wave function is a useful intermediate step in computations of observables, and can be seen as a way to modularize the calculations.

We will calculate the wave function from Faddeev amplitudes determined by Faddeev equations. Our approach for the ground state is similar to the one of Canham and Hammer in Ref. [15], where two-neutron halos were described as three-body systems with  $s$ -wave interactions in Halo EFT. However, we go beyond the treatment of Ref. [15] since we do not assume that the spin of  $^9\text{Li}$  and the total angular momentum of the  $^{11}\text{Li}$  bound state are both zero. Instead we analyze the spin structure of  $^{11}\text{Li}$  in detail.

### A. Jacobi momenta and Faddeev equations

Before discussing the Faddeev equations through which we calculate the ground state wave function and introducing the different interactions therein, we first summarize how the different momenta in the three-body system can be described. Typically Jacobi momenta are employed, whereby the system is described in terms of a relative momentum within a two-body subsystem and the momentum between the third particle and the subsystem. The third particle is called the spectator. Since there are three different choices of spectator possible there are three different Jacobi co-ordinate systems and these are labeled by the particle chosen as spectator. The definition of the Jacobi momenta  $\mathbf{p}_i$  and  $\mathbf{q}_i$  with respect to spectator  $i$  in a system with masses  $\{m_i, m_j, m_k\}$  and momenta  $\{\mathbf{k}_i, \mathbf{k}_j, \mathbf{k}_k\}$  reads

$$\mathbf{p}_i := \mu_{jk} \left( \frac{\mathbf{k}_j}{m_j} - \frac{\mathbf{k}_k}{m_k} \right), \quad \mathbf{q}_i := \mu_{i(jk)} \left( \frac{\mathbf{k}_i}{m_i} - \frac{\mathbf{k}_j + \mathbf{k}_k}{M_{jk}} \right). \quad (1)$$

The Faddeev equations for the abstract Faddeev components  $|F_i\rangle$  can be written as

$$|F_i\rangle = \sum_{j \neq i} G_0 t_j |F_j\rangle, \quad (2)$$

where  $G_0$  is the free Green's function and  $t_j$  is the two-body  $t$ -matrix for the  $(ik)$  sub-system, embedded in the three-body Hilbert space. The concrete expression in the case of a two-neutron system with one  $nn$  and one  $nc$  interaction reads

$$F_c(q) = \left( 1 + (-1)^{l(\zeta_c) + s(\xi_c)} \right) \int dq' q'^2 X_{cn}(q, q') 4\pi \tau_n(q') {}_c\langle \xi_c | \xi_n \rangle_n F_n(q'), \quad (3)$$

$$F_n(q) = {}_n\langle \xi_n | \xi_c \rangle_c \int dq' q'^2 X_{nc}(q, q') 4\pi \tau_c(q') F_c(q') - {}_n\langle \xi_n | \mathcal{P}_{nn}^{(\text{spin})} | \xi_n \rangle_n \int dq' q'^2 X_{nn}(q, q') 4\pi \tau_n(q') F_n(q'). \quad (4)$$

whereby the functions  $F_i(q)$  are related to the abstract components  $|F_i\rangle$  via  $F_i(q) := \int dp p^2 g_{l(\zeta_i)}(p) {}_i\langle p, q; \zeta_i | F_i \rangle$  with some orbital angular momentum quantum numbers  $\zeta_i$ . The regulators are given by the  $g_l$ . The  $X_{ij}$  are the so-called “kernel functions” originating from the evaluation of free Green's functions between states differing in the spectator.

The expressions can be found in Ref. [2]<sup>2</sup>. The functions  $\tau_i$  are related to t-matrix elements and will be defined in Eq. (20). A three-body force can be included in these Faddeev equations by replacing  $X_{nn}(q, q')$  by  $X_{nn}(q, q') + h$  with  $h$  being some three-body force parameter, see, e.g., Ref. [2]. Here the multiindex  $\xi_n$  specifies the spin state of the three-body system seen from the neutron as spectator when the  $nc$  subsystem is in the spin state of the  $nc$  interaction channel. Analogously,  $\xi_c$  specifies the spin state seen from the core as spectator when the  $nn$  subsystem is the the spin state of the  $nn$  interaction channel<sup>3</sup>. In the case of a spinless core these overlaps read

$${}_n\langle \xi_n | \xi_c \rangle_c = -1, \quad (5)$$

$${}_n\langle \xi_n | \mathcal{P}_{nn}^{(\text{spin})} | \xi_n \rangle_n = -1, \quad (6)$$

and one obtains Faddeev equations equivalent to the ones from Ref. [15]: the equations are the same apart from a relative minus sign in the definition of  $F_c$  from the  $F_n$  between our version and the one from Ref. [15]. If one continues this comparison to the level of wave functions, one finds that the total wave functions are equivalent up to overall minus signs that depend on the spectator and are not observable: in the case of  $\Psi_c(p, q)$  there is a relative minus sign, while in the case of  $\Psi_n(p, q)$  there is no sign difference.

## B. Spin structure of the interactions and of $^{11}\text{Li}$

Now that we have seen the Faddeev equations and the way they are influenced by spin states, we want to discuss the spin structure of the interactions specified as t-matrices as well as the overall spin structure of the two-neutron halo in detail.  $^{11}\text{Li}$  and  $^9\text{Li}$  have the same non-zero overall angular momentum:  $J = s_c = 3/2$ . This makes the  $nc$  dynamics more complicated, since the neutron and  $^9\text{Li}$  can interact in either the spin-1 or spin-2 channel.

We treat the core spin in two different ways:

- In Appendix A, we show that if the  $nc$  interactions in both the spin-1 and spin-2 channels have the same strength then the three-body Hamiltonian can be separated into two terms. In one the  $nn$  system is in a spin-0 configuration and in the other the two neutrons form a spin-1 pair. The interactions in the first Hamiltonian are the same as those in the Hamiltonian that treats the  $^9\text{Li}$  and  $^{11}\text{Li}$  as spin-0 particles. Therefore in this case we can just carry out a calculation that neglects the core spin, since that quantum number does not play a role in the dynamics of the system. For the ground state we explicitly checked the equivalence of the calculation having two  $nc$  spin channels of equal interaction strength with the spinless calculation<sup>4</sup> by verifying that the numerical results for the wave functions were the same. Note that this equivalence statement only refers to the spatial parts. If one wants to assemble the full state, the spatial solution has to be combined with the correct spin state.
- In the other approach, we take the core spin into account and assume that the leading-order  $nc$  interaction is only in the  $s_c + 1/2$  (spin-2) channel. The interaction in the  $s_c - 1/2$  (spin-1) channel is taken to be subleading.

Previous Halo EFT treatments basically used the first approach, whereby Appendix A can be seen as a formalization of an argument given in Ref. [2].

We now describe the spin configurations. We focus on the case with the  $nc$  interaction in the  $s_c + 1/2$  channel and mention the simplifications when the case with two equal  $nc$  interactions is realized through a calculation taking  $s_c = 0$ . For specifying the interaction channels in the three-body system we use a basis of states of definite  $L$  and  $S$  but in general indefinite  $J$ . The interaction channel for the  $nn$  interaction, which is given by the conditions  $l = 0$  and  $s = 0$  (seen from core) can be written as

$$|(0, \lambda) \lambda, \mu\rangle_c \left| \left(0, \frac{3}{2}\right) \frac{3}{2}, M_S \right\rangle_c \quad (7)$$

where the core is used as the spectator. Here we have specified the states in  $LS$ -coupling, using the following notation:  $|(l, \lambda) L, M_L\rangle_i |(s, \sigma) S, M_S\rangle_i$ , where the total orbital angular momentum of the three-body system  $\mathbf{L} = \mathbf{l} + \boldsymbol{\lambda}$ , with  $\mathbf{l}$

<sup>2</sup> We use the definition  $X_{ij}(q, q') := \int dp p^2 \int dp' p'^2 g_{l(\zeta_i)}(p) g_{l(\zeta_j)}(p') {}_i\langle p, q; \zeta_i | G_0 | p', q'; \zeta_j \rangle_j$ . In the case of sharp-cutoff regularization via the  $g_l$  these can be neglected at low momenta. If additionally the already mentioned interaction channels are  $s$ -wave, one can use the expressions from Ref. [2]. The notation is slightly different, whereby the relation  $X_{nc}(q, q') = -m_n X_{00}^n(q, q'; B_3)$  holds. Moreover, the relation  $X_{cn}(q, q') = X_{nc}(q', q)$  can be employed. The function  $X_{nn}$  has a  $\mathcal{P}_{nn}^{(\text{spatial})}$  in front of the  $G_0$ . Here the relation  $X_{nn}(q, q') = -m_n X_{00}^c(q, q'; B_3)$  can be used. Alternatively, the regulator effects on the kernel functions could be explicitly taken into account by evaluating some of the integrals in the functions numerically. This is discussed for  $^6\text{He}$  in Ref. [39].

<sup>3</sup> Note the semantic difference between “specifies the spin state” and “is the spin state”: e.g.,  $\xi_c$  is just a collection of quantum numbers, denoted by an subscript  $c$ . If applied with the core as spectator, then this collection specifies the spin state of the  $nn$  interaction channel. I.e.,  $|\xi_c\rangle_c$  is the spin state of the  $nn$  interaction channel. Nevertheless  $\xi_c$  is just a collection of quantum numbers and can be also applied by using another spectator, which results in a different spin state. This means that  $|\xi_c\rangle_n$  is a mathematically valid expression. However, it is not necessarily an allowed spin state of this system (e.g.,  $|\xi_c\rangle_n$  would require neutrons of spin  $3/2$ ).

<sup>4</sup> We will sometimes call this calculation “spinless” for simplicity. However, this adjective refers only to the core and the overall halo nucleus. The spins of the neutrons are always included.

the orbital angular momentum of the  $jk$  subsystem and  $\lambda$  the orbital angular momentum of particle  $i$  relative to the  $jk$  pair. Similarly the total spin  $\mathbf{S}$  is composed of the spin of the pair plus the spin of the spectator:  $\mathbf{S} = \mathbf{s} + \boldsymbol{\sigma}$ . In the case where the core spin does play a role the  $nc$  pair interacts when  $l = 0$  and  $s = 2$  (seen from the spectator neutron), which can be written as

$$|(0, \lambda) \lambda, \mu\rangle_n \left| \left( 2, \frac{1}{2} \right) \frac{3}{2}, M_S \right\rangle_n, \quad (8)$$

where the neutron is used as spectator. Since for the ground-state calculation we restrict ourselves to  $L = 0$  it follows that  $S = 3/2$  has to hold so that the  $^{11}\text{Li}$  ground state has the correct angular momentum. The spins are not affected by the  $E1$  operator, but, in contrast, the  $L$  can change, which is why we want to consider both  $L = 0$  (bound state) and  $L = 1$  (scattering state created after action of electric dipole operator).

In the calculations where the core spin is neglected all the  $3/2$  have to be replaced by zeros and  $M = 0$  holds. This makes the transformation of the spin states between the different spectators simple:

$$|(0, 0) 0, 0\rangle_c = - \left| \left( \frac{1}{2}, \frac{1}{2} \right) 0, 0 \right\rangle_n. \quad (9)$$

Now, if the core spin is taken into account the corresponding relation reads

$$\left| \left( 0, \frac{3}{2} \right) \frac{3}{2}, M_S \right\rangle_c = -\frac{\sqrt{5/2}}{2} \left| \left( 2, \frac{1}{2} \right) \frac{3}{2}, M_S \right\rangle_n - \frac{\sqrt{3/2}}{2} \left| \left( 1, \frac{1}{2} \right) \frac{3}{2}, M_S \right\rangle_n. \quad (10)$$

Note that each first number following an opening round bracket is the spin quantum number of the subsystem originating from the coupling of the subsystem spins. In the case of the core of spectator these are  $1/2$  and  $1/2$ , while in the case of the neutron spectator these are  $1/2$  and  $3/2$ .

As an approximation we take only the following partial-wave component of the  $^{11}\text{Li}$  ground state into account

$$\left| (0, 0) 0 \left( 0, \frac{3}{2} \right) \frac{3}{2}; \frac{3}{2}, M \right\rangle_c = |(0, 0) 0, 0\rangle_c \left| \left( 0, \frac{3}{2} \right) \frac{3}{2}, M \right\rangle_c, \quad (11)$$

which was easily recoupled from  $jJ$ -coupling into  $LS$ -coupling. In  $jJ$ -coupling we use the following notation:  $|(l, s) j(\lambda, \sigma) J; J, M\rangle_i$ . Again, the relation for the spinless case is obtained by replacing the  $3/2$  in Eq. (11) by zeros.

In order to refer to certain partial-wave states compactly, we use multiindices. We use the following naming convention here: multiindices specifying a full state in  $jJ$ -coupling are denoted by  $\Xi$ , multiindices denoting the pure spatial part are denoted by  $\zeta$ , and those denoting the spin part are denoted by  $\xi$ . We introduce the following abbreviations:

$$\Xi_c^{(M)} := (0, 0) 0 \left( 0, \frac{3}{2} \right) \frac{3}{2}; \frac{3}{2}, M, \quad (12)$$

$$\zeta_c := (0, 0) 0, 0, \quad (13)$$

$$\xi_c^{(M)} := \left( 0, \frac{3}{2} \right) \frac{3}{2}, M. \quad (14)$$

Using these Eq. (11) can be written as

$$\left| \Xi_c^{(M)} \right\rangle_c = \left| \zeta_c \right\rangle_c \left| \xi_c^{(M)} \right\rangle_c. \quad (15)$$

Moreover, we will use the definition  $\xi_n^{(M)} := (2, \frac{1}{2}) \frac{3}{2}, M$  for describing the calculations with only one  $nc$  interaction channel.

### C. Spatial structure of the interactions

Now that we have discussed the spin structure of the interactions as well as of  $^{11}\text{Li}$ , we have to discuss the general nature of the interactions. For our EFT calculation it is particularly useful to use the interactions in the form of

t-matrices, as in their denominators the different order terms can be identified. The leading-order reduced t-matrix of the  $nn$  interaction reads

$$\tau_{nn}(E) = \frac{1}{4\pi^2\mu_{nn}} \frac{1}{1/a_{nn} + ik}, \quad (16)$$

whereby  $a_{nn}$  is the  $nn$  scattering length and the relation  $k = \sqrt{2\mu_{ij}E}$  holds. The relation between the reduced t-matrix matrix element and the full two-body t-matrix element is

$$\langle p, l, s | t_{ij}(E) | p', l', s' \rangle = 4\pi \delta_{l,l'} \delta_{s,s'} \delta_{l_{ij},l} \delta_{s_{ij},s} g_{l_{ij}}(p) \tau_{ij}(E) g_{l_{ij}}(p'). \quad (17)$$

The  $nc$  interaction is given at leading order by the  $s$ -wave virtual state<sup>5</sup> characterized by the virtual state energy. The t-matrix reads

$$\tau_{nc}(E) = \frac{1}{4\pi^2\mu_{nc}} \frac{1}{\gamma_{nc} + ik}. \quad (18)$$

The virtual state momentum  $\gamma_{nc}$  is related to the virtual state energy  $E_{nc}$  according to  $\gamma_{nc} = -\sqrt{2\mu_{nc}E_{nc}}$ .

The embedding of the t-matrices in the three-body space is given by

$${}_i \langle p, q; \zeta, \xi | t_i(E_3) | p', q'; \zeta', \xi' \rangle_i = \delta_{\zeta,\zeta'} \delta_{\xi,\xi'} \langle p, l(\zeta), s(\xi) | t_{jk} \left( E_3 - \frac{q^2}{2\mu_{i(jk)}} \right) | p', l(\zeta'), s(\xi') \rangle \frac{\delta(q - q')}{q'^2}. \quad (19)$$

This motivates the introduction of

$$\tau_i(q; E_3) := \tau_{jk} \left( E_3 - \frac{q^2}{2\mu_{i(jk)}} \right), \quad (20)$$

for compact notation. The three-body energy  $E_3$  is in our case given by  $-B_3 = -S_{2n}$ . Sometimes this second argument of  $\tau_i$  is omitted.

#### D. From the Faddeev amplitudes to wave functions

Now that we have discussed the Faddeev equations and the effective interactions that appear in them, we turn our attention to the wave function and how it is obtained from the Faddeev amplitudes. The starting point is the relation between the abstract Faddeev amplitudes  $|F_i\rangle$  and the overall state  $|\Psi\rangle$ . It is given by

$$|\Psi\rangle = \sum_i G_0 t_i |F_i\rangle. \quad (21)$$

We can now define individual Faddeev components of the wave function that appear here as

$$\psi_i(p, q) = G_0^{(i)}(p, q; E_3) 4\pi \tau_i(q; E_3) F_i(q).$$

By projecting on a reference state and using the representations of the Faddeev amplitudes one obtains the overall wave function in a particular partial wave specified in terms of a spatial multiindex  $\zeta$  and a spin multiindex  $\xi$  as:

$$\begin{aligned} \Psi_{c;\zeta,\xi}(p, q) &= \sum_{M'} \psi_c(p, q) \delta_{\zeta,\zeta_c} \delta_{\xi,\xi_c^{(M')}} + \sum_{M'} \left( 1 + (-1)^{l-s} \right) \delta_{L,0} \delta_{M_L,0} \delta_{\lambda,l} \frac{\sqrt{2l+1}}{2} (-1)^l \\ &\times \left\langle \xi \left| \xi_n^{(M')} \right\rangle_n \int_{-1}^1 dx P_l(x) \psi_n(\kappa_{cnp}(p, q, x), \kappa_{cnq}(p, q, x)). \end{aligned} \quad (22)$$

It turns out that in our case

$$\Psi_c(p, q) := \left\langle p, q; \Xi_c^{(M)} \right| \Psi \rangle = \left\langle p, q; \zeta_c, \xi_c^{(M)} \right| \Psi \rangle, \quad (23)$$

---

<sup>5</sup> Note that the atomic mass evaluation [19, 40] characterizes this state as an  $s$ -wave resonance. In principle the effective nuclear  ${}^9\text{Li}-n$   $s$ -wave potential could have a barrier that produces a low-energy resonance. However, the main references given by the atomic evaluation in Ref. [40] characterize this state as a virtual state [41, 42]. We follow the original references.

with the multi-index defined as in Eqs. (12), is the most important partial-wave component of the wave function. Moreover, the quantum number  $M$  is undetermined, as the results are independent of  $M$ . (The superscript  $M$  of the multiindex  $\Xi_c$  is therefore omitted hereafter for brevity.) The expression obtained from Eq. (22) for this piece of the wave function is:

$$\Psi_c(p, q) = \psi_c(p, q) + {}_c\langle \xi_c | \xi_n \rangle_n \int_{-1}^1 dx P_0(x) \psi_n(\kappa_{cnp}(p, q, x), \kappa_{cnq}(p, q, x)). \quad (24)$$

This is the piece of the wave function considered by Canham and Hammer in Ref. [15].

We also checked the importance of wave function components corresponding to higher angular momenta for both the  $nn$  pair and the core relative to that pair, i.e.,

$$\Psi_c^{(l)}(p, q) := {}_c\langle p, q; \zeta_c^{(l)}, \xi_c | \Psi \rangle, \quad (25)$$

with the multiindex  $\zeta_c^{(l)} := (l, l) 0, 0$ . Our calculations show that  $\Psi_c^{(2)}$  is typically suppressed by a factor of 100 or more compared to  $\Psi_c$  in terms of their respective maxima. This means that here, as was done in Ref. [15], we will use only the  $l = 0$  states as reference states.

Moreover, all these equations are under the assumption that only  $L = 0$  states appear in the bound-state wave function. Because the core has spin  $3/2$  it is in principle possible for  $L = 2$  components to also be present in the  $J = 3/2^-$   $^{11}\text{Li}$  ground state. However, the leading-order three-body force in Halo EFT is operative only for  $L = 0$ : three-body forces that mix angular momenta or are operative in other  $L$  channels occur in Halo EFT, but only at higher orders. Therefore Halo EFT predicts a  $^{11}\text{Li}$  state with only  $L = 0$  (at leading order). In the case of  $L = 0$  and only  $s$ -wave interactions it is no loss of generality to assume that  $t_i$  projects also on  $L = 0$  and on  $\lambda = 0$ . In the spin space, we project not only in  $s$  but also in  $\sigma$  with no loss of generality.

Before presenting our results, we briefly discuss the parameters and renormalization conditions applied in our calculation. The  $^9\text{Li}$ - $n$  virtual state, whose nature was already discussed, is characterized by an energy of  $E_{nc} = 26(13)$  keV [19]. We use it to calculate a virtual-state momentum  $\gamma_{nc} = -\sqrt{2\mu_{nc}E_{nc}}$ . This parameterizes the  $nc$  interaction. The corresponding scattering length  $a_{nc}$  amounts to -29.8 fm. The  $nn$  interaction is parameterized by  $a_{nn} = -18.7$  fm [43]. Meanwhile, we use the two-neutron separation energy  $S_{2n} = 0.369$  MeV [19] to renormalize the three-body energy. The mass of the  $^9\text{Li}$  core is approximated by  $Am_n$  with the neutron mass  $m_n$  and  $A = 9$ . The two-body systems as well as the three-body system are regulated using sharp cutoffs. Moreover, the three-body cutoff  $\Lambda$  is chosen to be equal to the two-body cutoff,  $\Lambda = 400$  MeV. In order to check the convergence of the results, we compare to calculations with  $\Lambda = 300$  MeV and two thirds of the mesh points for discretizations and integrations.

### E. Radius of $^{11}\text{Li}$

The matter radius  $r_c$  which is the distance between the core and the halo's center of mass can be extracted as root-mean-square (rms) radius from the so-called form factor  $\mathcal{F}_c$  via

$$\langle r_c^2 \rangle = -6 \frac{d\mathcal{F}_c(k^2)}{dk^2} \Big|_{k^2=0} \left( \frac{2}{A+2} \right)^2. \quad (26)$$

The factor  $2/(A+2)$  stems from the conversion between the distance  $y_c$ , which corresponds to the momentum  $q_c$ , and  $r_c$ . The expression for the form factor reads [2]

$$\mathcal{F}_c(k^2) = \int dp dq p^2 q^2 \Psi_c^*(p, q) \Psi_c(p, q + k). \quad (27)$$

We use only the  $l = 0$  component of the wave function in our calculations, since, as discussed above, other components are suppressed by at least a factor of 100. This way we obtain  $\sqrt{\langle r_c^2 \rangle} = 0.87$  fm with a numerical uncertainty of roughly 0.02 fm and LO EFT uncertainty of approximately  $\sqrt{\langle r_c^2 \rangle} \sqrt{S_{2n}/E^*} \approx 0.32$  fm. Hereby, the two-neutron separation energy of  $^{11}\text{Li}$  is given by  $S_{2n}$  and the excitation energy of  $^9\text{Li}$  is given by  $E^*$ . In order to compare our value with experimental data we use the experimental values for the rms charge radii of  $^9\text{Li}$  and  $^{11}\text{Li}$ ,  $\sqrt{\langle r_9^2 \rangle}$  and  $\sqrt{\langle r_{11}^2 \rangle}$  from which  $\langle r_c^2 \rangle$  can be obtained. These can be obtained from isotope shift measurements. The first values were obtained in Ref. [44], while we use the more current ones from Ref. [21]. These yield<sup>6</sup>  $\sqrt{\langle r_c^2 \rangle} = \sqrt{\langle r_{11}^2 \rangle - \langle r_9^2 \rangle} = 1.04 \pm 0.14$  fm. If

<sup>6</sup> The commonly used relation  $\langle r_c^2 \rangle + \langle r_9^2 \rangle = \langle r_{11}^2 \rangle$  can be explained in terms of the factorization of the halo's electric form factor into the electric form factors of  $^9\text{Li}$  itself and of  $^9\text{Li}$  relative to the two neutrons with the latter then calculated with a point core. This factorization will break at higher orders in the EFT expansion when two- and higher-body currents enter. The size of such corrections is also governed by the power counting of halo EFT.



we also include the mean-square neutron charge radius,  $\langle r_n^2 \rangle = -0.1161 \pm 0.0022 \text{ fm}^2$  [45], we obtain  $\sqrt{\langle r_c^2 \rangle} = 1.08 \pm 0.14 \text{ fm}$  by using the formula from Ref. [46]. Our theoretical result is in good agreement with both values.

Furthermore, it is interesting to use our  $\sqrt{\langle r_c^2 \rangle}$  together with the  $\sqrt{\langle r_9^2 \rangle}$  from experiment to calculate an  $\sqrt{\langle r_{11}^2 \rangle}$ . We obtain  $\sqrt{\langle r_{11}^2 \rangle} = \sqrt{\langle r_c^2 \rangle + \langle r_9^2 \rangle} = 2.41 \pm 0.13 \text{ fm}$  (including the rms neutron charge radius changes the result by less than 0.02 fm). Our value is not far from the experimental result of  $2.48 \pm 0.04 \text{ fm}$  and agrees within uncertainties. This means that a LO EFT three-body description of  $^{11}\text{Li}$  is able to describe the charge radius without explicitly including core excitation. It will be interesting to see if this persists at NLO. Finally, we want to mention that  $r_c$  is related to the neutron-pair-to-core distance  $r_{c(nn)}$  by  $11 r_c/2 = r_{c(nn)}$ . Thereby we obtain for  $\langle r_{c(nn)}^2 \rangle^{1/2}$  a value of 4.8 fm with an LO EFT uncertainty of 1.8 fm. This large  $nn - c$  distance is another strong manifestation of the halo structure of  $^{11}\text{Li}$ .

### III. E1 COULOMB DISSOCIATION

In this section, we investigate the  $E1$  strength function without final-state interactions (FSIs) as well as the impact that  $nn$  and  $nc$  FSI separately have on this strength function. Before showing and discussing the results, we give a diagrammatic overview of these calculations in terms of the Feynman diagrams for the matrix elements of the  $E1$  operator. The diagrams are shown in Fig. 1. Final-state interactions are those interactions happening after the  $E1$  breakup of the halo nucleus. (In this section, only one FSI will be included at a time. The inclusion of multiple interactions at once will be discussed in the following section.)

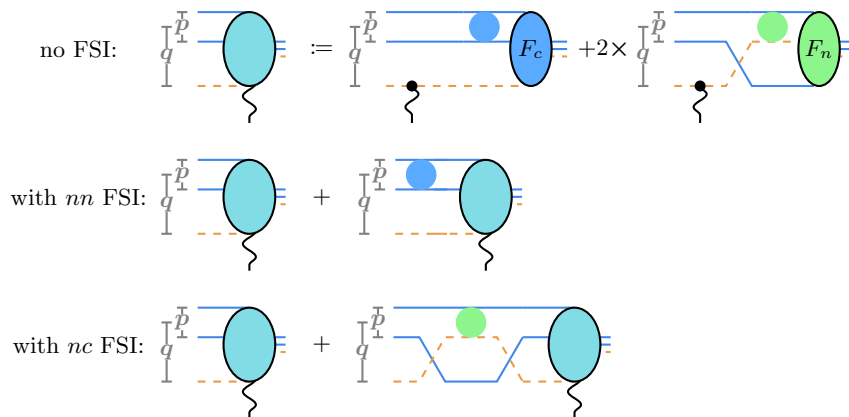


Figure 1. Diagrammatic representation of the  $E1$  matrix elements of distributions differing in the included FSIs. The neutrons are represented by blue solid lines and the  $^9\text{Li}$  core is represented by an orange dashed line. The first row describes the matrix element without FSI, whereby the ellipse with the external line on the left side represents the complete matrix element resulting from the action of the  $E1$  operator on the ground state. On the right-hand side of the first row this is made more explicit: The  $E1$  photons are represented by wiggly lines and the ground state is composed from its Faddeev amplitudes represented by ellipses with corresponding labels. The  $nn$  and  $nc$   $t$ -matrices are represented by circles. The second row shows the contributions for the matrix element that includes  $nn$  FSI, while the third row describes the matrix element with  $nc$  FSI.

While they modify the shape of the  $E1$  distribution, the integral over the distribution, i.e., the overall  $E1$  strength, is conserved according to a sum rule and therefore is not affected by FSIs. First we explain how this sum rule comes about.

#### A. The non-energy-weighted sum rule

The cumulative  $E1$  strength  $B(E1)(E)$  is defined as the integral of the  $E1$  strength up to an energy  $E$ .

$$B(E1)(E) := \int_0^E dE' \frac{dB(E1)}{dE'}. \quad (28)$$

According to the non-energy weighted sum rule (see, e.g., Ref. [47]) the total strength, i.e., integrated all the way to infinite energy, is related to the RMS-radius  $\sqrt{\langle r_c^2 \rangle}$  by

$$\lim_{E \rightarrow \infty} B(E1)(E) = \frac{3}{4\pi} Z_c^2 e^2 \langle r_c^2 \rangle. \quad (29)$$

This sum rule is derived using only the identity  $r_c^2 = \vec{r}_c \cdot \vec{r}_c$  and the completeness of the intermediate states. Therefore any approximate treatment of FSI should produce a cumulative distribution that has the same asymptotic value as that obtained when FSI is neglected, and that value should also be consistent with the  $\langle r_c^2 \rangle$  computed using the bound-state wave function.

### B. $E1$ strength distribution without FSI

Our explicit expression for obtaining the  $E1$  strength of the  $2n$  halo nucleus with the ground state  $|\Psi\rangle$  reads

$$\frac{dB(E1)}{dE} = e^2 Z_c^2 \sum_{\mu} \int dp dq p^2 q^2 \left| \left\langle p, q; \zeta_c^{(1,\mu)}, \xi_c \left| r_c Y_{1\mu}(\mathbf{r}_c) P_{\Xi_c} \right| \Psi \right\rangle \right|^2 \delta \left( E - \frac{p^2}{2\mu_{nn}} - \frac{q^2}{2\mu_{c(nn)}} \right), \quad (30)$$

where we applied the approximation of using only the  $|\Xi_c\rangle_c$  partial-wave component. This is realized by inserting the corresponding projection operator  $P_{\Xi_c}$ . It results in the omission of the  $l \neq 0$  components (see Eq. (25)). This should be a good approximation since, as discussed above, the higher- $l$  components are suppressed by a factor of at least 100. The orbital angular momentum quantum numbers after the breakup are collected in the multiindex  $\zeta_c^{(1,\mu)}$ , which is given by  $\zeta_c^{(1,\mu)} = (0, 1) 1, \mu$ . Note that we do not have to explicitly average over  $M$  in Eq. (30) as the initial state is independent of it. Working in the  $c$ -representation for the wave function  $|\Psi\rangle$  and retaining only the dominant component  ${}_c\langle p, q; \zeta_c, \xi_c | \Psi \rangle$  it is straightforward to evaluate the operator  $r_c Y_{1\mu}(\mathbf{r}_c)$  in the plane-wave basis. This produces the concrete relation that is implemented:

$$\frac{dB(E1)}{dE} = \frac{3e^2 Z_c^2}{4\pi} \left( \frac{2}{A+2} \right)^2 \int_0^{\sqrt{2\mu_c E}} dq q^2 \sqrt{2\mu_{nn}^3} \sqrt{E - \frac{q^2}{2\mu_c}} \left| \partial_{q'} \Psi_c \left( \sqrt{2\mu_{nn}} \left( E - \frac{q^2}{2\mu_c} \right), q' \right) \right|_{q'=q}^2, \quad (31)$$

where  $A$  is the mass number of the core and  $\mu_c := \mu_{c(nn)}$  holds. The wave function  $\Psi_c(p, q)$  is obtained from the Faddeev amplitudes as described in the previous section.

### C. Including $nn$ FSI

The dipole strength can also be calculated straightforwardly with  $nn$  final state interactions (FSI) taken into account. This is done by inserting the Møller [48, 49] operator of the  $nn$  interaction  $\Omega_{nn}^\dagger$  right before the final state:

$$\frac{dB(E1)}{dE} = e^2 Z_c^2 \sum_{\mu} \int dp dq p^2 q^2 \left| \left\langle p, q; \zeta_c^{(1,\mu)}, \xi_c \left| \Omega_{nn}^\dagger r_c Y_{1\mu}(\mathbf{r}_c) P_{\Xi_c} \right| \Psi \right\rangle \right|^2 \delta \left( E - \frac{p^2}{2\mu_{nn}} - \frac{q^2}{2\mu_c} \right). \quad (32)$$

The Møller operator  $\Omega_{nn}^\dagger$  is given by

$$\Omega_{nn}^\dagger = \mathbb{1} + \int dp dq p^2 q^2 \left( |p, q\rangle_c {}_c\langle p, q| \otimes \mathbb{1}^{(\text{orbital})} \otimes \mathbb{1}^{(\text{spin})} \right) t_{nn}(E_p) G_0^{(nn)}(E_p). \quad (33)$$

It converts the free state  ${}_c\langle p, q; \zeta_c^{(1,\mu)}, \xi_c |$  into the product of an  $nn$  distorted wave and a plane-wave associated with the Jacobi momentum of the core relative to the  $nn$  pair at  $t = 0$ . The time-evolved version of the resulting three-body state has  ${}_c\langle p, q; \zeta_c^{(1,\mu)}, \xi_c | e^{iH_0 t}$  as an asymptotic state for  $t \rightarrow \infty$ .<sup>7</sup> The inclusion of  $\Omega_{nn}^\dagger$  therefore ensures that the state obtained after the action of the  $E1$  operator is overlapped with the three-body scattering state that includes  $nn$  FSI, so leading to an  $E1$  distribution in which the effects of  $nn$  FSI are included.

<sup>7</sup> The Møller operator thus makes use of the asymptotic condition, which requires that every state in the Hilbert space  $\mathcal{H}$  of solutions of a Schrödinger equation can form the asymptote of some scattering state, see e.g. Ref. [48].

Since  $\Omega_{nn}^\dagger$  is an identity in the momentum of the spectator,  $q$ , and in the associated parts of the partial wave states, it commutes with the  $E1$  operator  $r_c Y_{1\mu}(\mathbf{r}_c)$ . This means that this calculation is an easy extension of the one described in the previous subsection. One obtains Eq. (31) where  $\Psi_c$  is replaced by the wave function including  $nn$  FSI:

$$\Psi_c^{(\text{wFSI})}(p, q) := {}_c \langle p, q; \zeta_c, \xi_c | \left( \mathbb{1} + t_{nn}(E_p) G_0^{(nn)}(E_p) \right) | \Psi \rangle. \quad (34)$$

An explicit expression is given in Eqs. (35, 36) of Ref. [50]. While the nucleus considered in Ref. [50] is  ${}^6\text{He}$ , the corresponding equations apply here as well, as they only describe the inclusion of  $nn$  FSI.

#### D. Including $nc$ FSI

The distribution with  $nc$  FSI can be obtained in a similar fashion as the distribution with  $nn$  FSI. The Møller operator  $\Omega_{nn}^\dagger$  has to be replaced by  $\Omega_{nc}^\dagger$ , which is given by

$$\Omega_{nc}^\dagger = \mathbb{1} + \int dp dq p^2 q^2 \left( |p, q\rangle_n {}_n \langle p, q| \otimes \mathbb{1}^{(\text{orbital})} \otimes \mathbb{1}^{(\text{spin})} \right) t_{nc}(E_p) G_0^{(nc)}(E_p). \quad (35)$$

However, because  $\Omega_{nc}^\dagger$  does not commute with the  $E1$  operator, multiple three-body bases have to be used in the evaluation of Eq. (35). An explicit expression for the distribution with  $nc$  FSI will be given below.

#### E. Results

We now show our results for the  $E1$  strength distributions from calculations with the two  $nc$  interaction channels ( $s=1$  and  $s=2$ ). For the spatial part of the solution, we employed the equivalence statement described in Appendix A, i.e., we did an calculation with core spin and overall spin set to zero.

The results for the  $E1$  distributions with no FSI as well with either a single  $nn$  or  $nc$  FSI are shown in the left-hand panel of Fig. 2. In the right panel, we show the cumulative distribution  $B(E1)(E)$ .

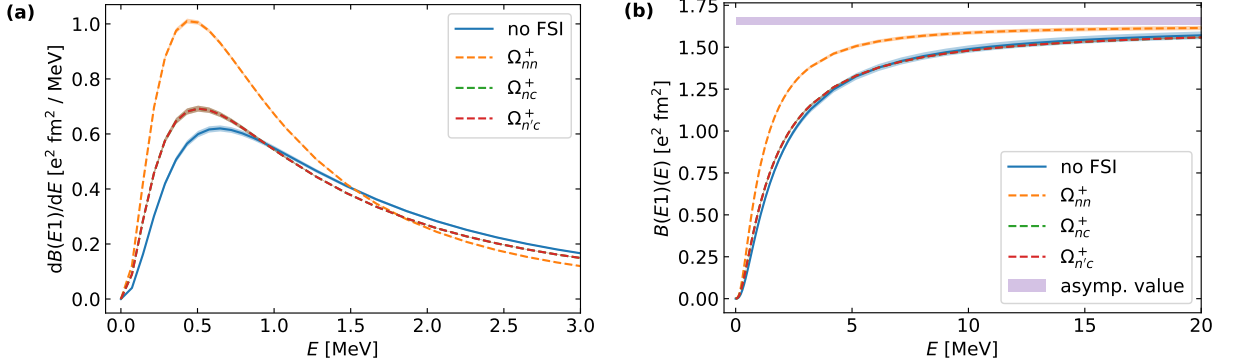


Figure 2. The left panels (a) shows  $E1$  strength distributions of  ${}^{11}\text{Li}$  with different FSIs included. The right panel (b) shows the corresponding cumulative  $E1$  strength distributions. Numerical uncertainties are indicated by bands, which are very narrow here. They were obtained by comparing the calculations with ones having roughly two thirds as many mesh points and a cutoff of three fourths of the original one.

It can be seen that the  $nn$  FSI influences the shape of the strength distribution significantly, producing a strong enhancement at low energies, and a continuing depletion of the strength at higher energies.  $nc$  FSI (and  $n'c$  FSI) also increase the strength at low energy, but their influence is markedly less than that of the  $nn$  FSI.

In the case of the cumulative distributions a common asymptotic value can be observed, in accordance with the sum rule. We expect that the agreement would become even better if we continued the calculation to higher energies. The asymptotic values are also in approximate agreement with the overall  $E1$  strength value calculated from  $\langle r_c^2 \rangle$  computed in Sec. II E

### F. Role of $nc$ interaction channels in $^{11}\text{Li}$

Now that we have assessed the impact of FSI on the results, we want to compare the calculation with two  $nc$  interaction channels to that with only one  $nc$  interaction channel. The parameter describing the  $nc$  interaction  $E_{nc}$  was in both cases the same, the difference is that when only the  $s = 2$   $nc$  spin channel is active the interaction is switched off in the  $s = 1$   $nc$  spin channel. The results of the calculations are shown in Fig. 3. While the left panel contains the theoretical curves, the right panels contains the same distributions but folded with the detector resolution and compared with the experimental data. More information on the folding and the experimental data can be found in Section IV D.

Also shown there is a recent calculation of Hongo and Son for  $2n$  halo nuclei [51]. In this context, it is important to note that the universal curve from Hongo and Son is derived in an EFT picture of  $2n$ -halo nuclei in which they are bound by the  $nn$  interaction and a three-body force: the  $nc$  interaction is taken to be an NLO effect there. It therefore applies to  $2n$  halo nuclei where  $S_{2n}$  and  $\epsilon_n = \hbar^2/(2\mu_{nn}a_{nn}^2)$  are smaller than all other energy scales, and in particular smaller than  $\epsilon_{nc}$ . This is not the case in  $^{11}\text{Li}$  due to the near-threshold resonance in  $^{10}\text{Li}$ , and Hongo and Son themselves say the applicability of their results to  $^{11}\text{Li}$  is “doubtful”. Fig. 3 shows that the Hongo and Son calculation predicts a much lower  $E1$  strength than any of the calculations in which a low-energy  $nc$  virtual state plays a role in the structure of  $^{11}\text{Li}$ .

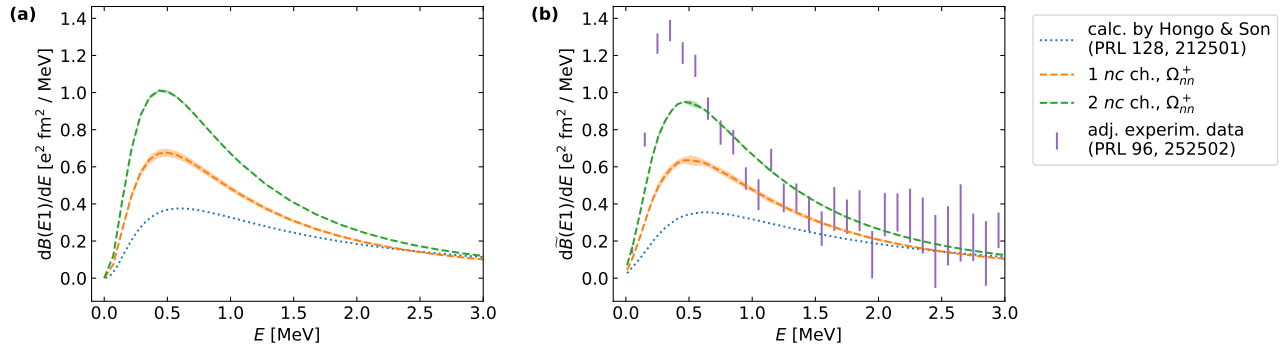


Figure 3.  $E1$  strength distributions with  $nn$  FSI included and different numbers of  $nc$  interaction channels for the ground state. We show the result by Hongo and Son [51] (blue), which corresponds to no  $nc$  interaction spin channels, in comparison with our results using one spin channel (orange) and two spin channels (green). The left panel (a) shows the theoretical curves. In the right panel (b) these distributions have been folded with the detector resolution and compared to the experimental data from Nakamura et al. [25] (adjusted to the current  $S_{2n}$  value).

Since  $nn$  FSI is included in all curves, they can directly be compared. It is clear that the low-energy strength increases with the number of  $nc$  interaction channels. The result by Hongo and Son [51] (blue curve) has too little strength for  $E \approx 0.5$  MeV. The calculation with one channel (orange curve) has already more strength, while using two channels (green curve) results in the highest strength. Since the  $nc$  interaction does not appear in any of the final-state-interaction treatments used here all the differences between the different results stem from effects in the initial-state  $^{11}\text{Li}$  nucleus. Crucially, all three calculations are adjusted to the same  $S_{2n}$ . It is then quite striking that the  $E1$  strength increases appreciably depending on the fraction of  $nc$  pairs that interact with a large  $nc$  scattering length: 0 of them, 5/8 of them, or all of them. (The factor of 5/8 is the ratio of the spin multiplicity of the  $nc$  interaction channel and the sum of multiplicities of all possible  $nc$  spin couplings, see Eq. (10).)

The description using two  $nc$  interaction channels, in which all the  $nc$  pairs in  $^{11}\text{Li}$  can scatter via a large  $a_{nc}$ , yields a much better description of the data in this leading-order calculation. Therefore we will use it for the investigations of the next section, where we seek to include effects due to both  $nn$  and  $nc$  FSI.

## IV. SUM-RULE PRESERVING APPROXIMATION SCHEMES FOR FSI

In this section, we explore different approximation schemes for the FSI in detail. Our goals are:

- (i) derive accurate approximation schemes for practical calculations, and
- (ii) understand the role of different FSI channels and orders in the multiple scattering series.

For this purpose, we make use of Møller operators, which were already briefly discussed in Section III C. The full final state can be written as

$${}_c\langle p, q; \Xi_f | \Omega_{nn+nc+n'c}^\dagger, \quad (36)$$

where  $\Xi_f$  is some set of orbital angular momentum and spin quantum numbers and  $\Omega_{nn+nc+n'c}^\dagger$  is the Møller operator containing all the two-body final-state interactions:

$$\Omega_{nn+nc+n'c} = \mathbb{1} + \int dp dq p^2 q^2 \sum_{\Xi} \frac{1}{E_{p,q} - H_0 - V_{nn} - V_{nc} - V_{n'c} - i\epsilon} (V_{nn} + V_{nc} + V_{n'c}) |p, q; \Xi\rangle {}_c\langle p, q; \Xi|. \quad (37)$$

Calculating the action of this operator on a plane-wave state is challenging due to the presence of three different two-body potentials,  $V_{nn}, V_{nc}, V_{n'c}$ . To obtain the three-body scattering state, we would have to solve the Faddeev (or equivalent) equations above three-body breakup. Therefore we are interested in approximation strategies, especially since comparing different approximations can lead to additional insights into the final-state dynamics. Note, however, that there are also calculations based on full three-body scattering states of  $^{11}\text{Li}$  available, see, e.g., Ref. [28].

We continue by analyzing the final scattering state in order to obtain approximations. Using the Faddeev equations for scattering states as an intermediate step produces

$${}_c\langle p, q; \Xi_f | \Omega_{nn+nc+n'c}^\dagger = {}_c\langle p, q; \Xi_f | \left( \mathbb{1} + \sum_i t_i G_0 + \sum_i t_i G_0 \sum_{j \neq i} t_j G_0 + \dots \right), \quad (38)$$

where we omitted the arguments of the t-matrices and Green's functions for brevity. From this the following approximation can be obtained:

$${}_c\langle p, q; \Xi_f | \left( \mathbb{1} + \sum_i t_i G_0 \right). \quad (39)$$

This treatment, which keeps the first-order terms in the multiple-scattering series, is not unitary. In contrast the Møller operators introduced in the previous section are isometric and unitary (since neither the  $nn$  nor the  $nc$  subsystem supports a bound state). Non-unitarity can lead to unphysical gains and losses of probability, which are manifest as violations of the non-energy-weighted sum rule.

In order to ensure we have a sum-rule-preserving approximation scheme, we propose to use products of Møller operators, whereby the single Møller operators correspond to single types of interactions ( $nn$  or  $nc$  or  $n'c$ ). This ensures that we keep unitarity-preserving combinations of terms in the multiple-scattering series. Of course, in doing so we do not truncate the multiple-scattering series at a given order in t-matrices, because it is not possible to do that and also maintain unitarity. Unitarity is only obtained in such a scheme if the multiple-scattering series is summed to infinite order.

### A. Organization of FSI calculations

We will now work out how to efficiently organize calculations of  $E1$  distributions with FSIs based on combinations of Møller operators. We will identify ingredients which different distributions have in common and describe the calculation of the different matrix elements on this basis. The procedure to obtain the final distributions from the matrix elements is then basically independent of included FSIs.

In proceeding in this way, it is useful to specify the initial and final states and to discuss their partial-wave structure. The initial state used in the calculations of this section is that obtained by acting with the  $E1$  operator on the  $\Xi_c := \zeta_c, \xi_c$  partial-wave component of the ground state:

$$|i\rangle := \mathcal{M}(E1, \mu) P_{\Xi_c} |\Psi\rangle. \quad (40)$$

After this  $E1$  transition (FSIs not yet included) the system is in the partial-wave state

$$\left| \zeta_c^{(1,\mu)}, \xi_c \right\rangle_c. \quad (41)$$

In order to compactly specify the final states after FSIs, which can be in various partial waves due to recoupling, we introduce multiindices for the spatial and for the spin part:

$$\left| \zeta_f^{(\bar{l}, \bar{\lambda}; \mu)} \right\rangle_c \left| \xi_f^{(\bar{s}; M)} \right\rangle_c := |(\bar{l}, \bar{\lambda}) 1, \mu\rangle_c \left| \left( \bar{s}, \frac{3}{2} \right) \frac{3}{2}, M \right\rangle_c \quad (42)$$

for the spin part. For illustrative purposes, we put the multiindices directly into kets, since they are usually used with the core as spectator. The quantum numbers here have bars on top in order to distinguish them from the ones characterizing the ground state. While overall spin and orbital angular momentum are conserved, the subsystem quantum numbers are in general not conserved.

In the case of the two  $nc$  interaction channels ( $s_c + 1/2$  and  $s_c - 1/2$ ), the Hamilton operator decouples into one with the  $nn$  system in spin 0 configuration and one with the  $nn$  system in spin 1 configuration. Therefore, the initial state with  $s = 0$  will remain in this configuration and we have  $\bar{s} = 0$ .

On this basis we define the following “ingredients”:

$$\mathcal{A}_{\bar{l}, \bar{\lambda}; \mu; \bar{s}, M}^{(1)}(p, q) := \left\langle p, q; \zeta_f^{(\bar{l}, \bar{\lambda}; \mu)}, \xi_f^{(\bar{s}; M)} \left| (\Omega_{nc}^\dagger - \mathbb{1}) \right| i \right\rangle, \quad (43)$$

$$\mathcal{A}_{\bar{l}, \bar{\lambda}; \mu; \bar{s}, M}^{(2)}(p, q) := \left\langle p, q; \zeta_f^{(\bar{l}, \bar{\lambda}; \mu)}, \xi_f^{(\bar{s}; M)} \left| (\Omega_{n'c}^\dagger - \mathbb{1}) (\Omega_{nc}^\dagger - \mathbb{1}) \right| i \right\rangle. \quad (44)$$

To evaluate these matrix elements we must recouple the partial-wave states (momenta, angular momenta, and spins) from the  $c$ -spectator basis to the  $n'$ -spectator basis in the case of  $\mathcal{A}_{\bar{l}, \bar{\lambda}; \mu; \bar{s}, M}^{(1)}(p, q)$ , and then, additionally from the  $n'$ -spectator basis to the  $n$ -spectator basis in the case of  $\mathcal{A}_{\bar{l}, \bar{\lambda}; \mu; \bar{s}, M}^{(2)}(p, q)$ . In both cases the final state is specified using the core as spectator implying another recoupling. The details of those calculations, together with explicit expressions for these matrix elements, are given in Appendix B and Appendix C respectively.

Once  $\mathcal{A}_{\bar{l}, \bar{\lambda}; \mu; \bar{s}, M}^{(1)}(p, q)$  and  $\mathcal{A}_{\bar{l}, \bar{\lambda}; \mu; \bar{s}, M}^{(2)}(p, q)$  have been calculated the related matrix elements  $\tilde{\mathcal{A}}_{\bar{l}, \bar{\lambda}; \mu; \bar{s}, M}^{(1)}(p, q)$  and  $\tilde{\mathcal{A}}_{\bar{l}, \bar{\lambda}; \mu; \bar{s}, M}^{(2)}(p, q)$  in which the roles of the two neutrons,  $n$  and  $n'$ , have been interchanged, can be found using the properties of the permutation operators  $\mathcal{P}_{nn}^{(\text{spatial})}$  and  $\mathcal{P}_{nn}^{(\text{spin})}$ . These yield the following relations between the  $\mathcal{A}$  and  $\tilde{\mathcal{A}}$  functions:

$$\tilde{\mathcal{A}}_{\bar{l}, \bar{\lambda}; \mu; \bar{s}, M}^{(1)}(p, q) = (-1)^{\bar{l}} (-1)^{-\bar{s}} \mathcal{A}_{\bar{l}, \bar{\lambda}; \mu; \bar{s}, M}^{(1)}(p, q), \quad (45)$$

$$\tilde{\mathcal{A}}_{\bar{l}, \bar{\lambda}; \mu; \bar{s}, M}^{(2)}(p, q) = (-1)^{-\bar{l}} (-1)^{-(1-\bar{s})} (-1) \mathcal{A}_{\bar{l}, \bar{\lambda}; \mu; \bar{s}, M}^{(2)}(p, q), \quad (46)$$

i.e., the tilde matrix elements are the same as the unbarred ones up to phase factors stemming from  $nn$  permutations.

Another important ingredient is the overlap of final and initial state with no “FSI operator” in between:

$$\mathcal{A}_\mu^{(0)}(p, q) \delta_{\bar{l}, 0} \delta_{\bar{\lambda}, 1} := \left\langle p, q; \zeta_f^{(\bar{l}, \bar{\lambda}; \mu)}, \xi_c^{(M)} \left| i \right\rangle. \quad (47)$$

This was already evaluated as part of the calculation of Eq. (31). This function depends on  $\mu$  but not on  $\bar{l}$ ,  $\bar{\lambda}$  and  $\bar{s}$ , since the overlap on the right is non-vanishing only if  $\bar{l} = 0$  and  $\bar{\lambda} = 1$  and  $\bar{s} = 0$ .

Using these ingredients, and the definition  $\tilde{\Omega}_{ij} := \Omega_{ij} - \mathbb{1}$ , we can obtain comparatively compact expressions for the matrix elements of different combinations of Møller operators.

First, we see that, with  $\mathcal{A}_\mu^{(0)}(p, q)$  in hand, the matrix element of the  $nn$  Møller operator, implicitly worked out in the previous section, is easily written as<sup>8</sup>:

$$\left\langle p, q; \zeta_f^{(\bar{l}, \bar{\lambda}; \mu)}, \xi_f^{(\bar{s}; M)} \left| \Omega_{nn}^\dagger \right| i \right\rangle = \left\langle p, q; \zeta_f^{(\bar{l}, \bar{\lambda}; \mu)}, \xi_f^{(\bar{s}; M)} \left| \left( \mathbb{1} + \int d\tilde{p} d\tilde{q} \tilde{p}^2 \tilde{q}^2 \sum_{\Omega} |\tilde{p}, \tilde{q}; \Omega\rangle_c \langle \dots | t_{nn}(E_{\tilde{p}}) G_0^{(nn)}(E_{\tilde{p}}) \right) \right| i \right\rangle \quad (48)$$

$$= \delta_{\bar{l}, 0} \delta_{\bar{\lambda}, 1} \delta_{\bar{s}, 0} \left( \mathcal{A}_\mu^{(0)}(p, q) + \frac{2}{\pi} g_0(p) \tau_{nn}(p) \int dp' p'^2 g_0(p') (p^2 - p'^2 + i\epsilon)^{-1} \mathcal{A}_\mu^{(0)}(p', q) \right) \quad (49)$$

$$=: \mathcal{B}_\mu(p, q) \delta_{\bar{l}, 0} \delta_{\bar{\lambda}, 1} \delta_{\bar{s}, 0}. \quad (50)$$

Then, since we also have a result for  $\tilde{\mathcal{A}}_{\bar{l}, \bar{\lambda}; \mu; \bar{s}, M}^{(1)}(p, q)$ , if we notate the action of the  $nn$  Møller operator to be the

<sup>8</sup> Note that  $\tau$  which is the “reduced t-matrix element” takes sometimes a momentum and sometimes an energy as argument in this paper. This variation stems from the context and there is no other reason.  $\tau_k(E)$  can be read as  $\tau_k(\sqrt{2\mu_{ij}E})$ .

$\mathcal{B}_\mu(p, q)$  defined in Eq. (50), we can write the matrix element of the product of the  $nn$  and  $nc$  Møller operators as:

$$\left\langle p, q; \zeta_f^{(\bar{l}, \bar{\lambda}; \mu)}, \xi_f^{(\bar{s}; M)} \left| \Omega_{nn}^\dagger \Omega_{nc}^\dagger \right| i \right\rangle = \left\langle p, q; \zeta_f^{(\bar{l}, \bar{\lambda}; \mu)}, \xi_f^{(\bar{s}; M)} \left| \left( \Omega_{nn}^\dagger + \tilde{\Omega}_{nc}^\dagger + \tilde{\Omega}_{nn}^\dagger \tilde{\Omega}_{nc}^\dagger \right) \right| i \right\rangle \quad (51)$$

$$= \delta_{\bar{l},0} \delta_{\bar{\lambda},1} \delta_{\bar{s},0} \mathcal{B}_\mu(p, q) + \mathcal{A}_{\bar{l}, \bar{\lambda}; \mu; \bar{s}, M}^{(1)}(p, q) + \delta_{\bar{l},0} \delta_{\bar{\lambda},1} \delta_{\bar{s},0} \frac{2}{\pi} g_0(p) \tau_{nn}(p) \int dp' p'^2 g_0(p') (p^2 - p'^2 + i\epsilon)^{-1} \mathcal{A}_{0,1;\mu;0,M}^{(1)}(p', q). \quad (52)$$

Finally, we can write the matrix element of a product of three Møller operators

$$\begin{aligned} \left\langle p, q; \zeta_f^{(\bar{l}, \bar{\lambda}; \mu)}, \xi_f^{(\bar{s}; M)} \left| \Omega_{nn}^\dagger \Omega_{n'c}^\dagger \Omega_{nc}^\dagger \right| i \right\rangle &= \delta_{\bar{l},0} \delta_{\bar{\lambda},1} \delta_{\bar{s},0} \mathcal{B}_\mu(p, q) + \left( 1 + (-1)^{\bar{l}+\bar{s}} \right) \mathcal{A}_{\bar{l}, \bar{\lambda}; \mu; \bar{s}, M}^{(1)}(p, q) \\ &+ 2\delta_{\bar{l},0} \delta_{\bar{\lambda},1} \delta_{\bar{s},0} \frac{2}{\pi} g_0(p) \tau_{nn}(p) \int dp' p'^2 g_0(p') (p^2 - p'^2 + i\epsilon)^{-1} \mathcal{A}_{0,1;\mu;0,M}^{(1)}(p', q) \\ &+ \mathcal{A}_{\bar{l}, \bar{\lambda}; \mu; \bar{s}, M}^{(2)}(p, q) + \delta_{\bar{l},0} \delta_{\bar{\lambda},1} \delta_{\bar{s},0} \frac{2}{\pi} g_0(p) \tau_{nn}(p) \int dp' p'^2 g_0(p') (p^2 - p'^2 + i\epsilon)^{-1} \mathcal{A}_{0,1;\mu;0,M}^{(2)}(p', q), \end{aligned} \quad (53)$$

where we also used Eq. (45). In the case of Eq. (53) the relation

$$\Omega_{nn}^\dagger \Omega_{n'c}^\dagger \Omega_{nc}^\dagger = \left( \mathbb{1} + \tilde{\Omega}_{nn}^\dagger \right) \left( \mathbb{1} + \tilde{\Omega}_{n'c}^\dagger \right) \left( \mathbb{1} + \tilde{\Omega}_{nc}^\dagger \right) \quad (54)$$

$$= \Omega_{nn}^\dagger + \left( \tilde{\Omega}_{n'c}^\dagger + \tilde{\Omega}_{nc}^\dagger \right) + \tilde{\Omega}_{nn}^\dagger \left( \tilde{\Omega}_{n'c}^\dagger + \tilde{\Omega}_{nc}^\dagger \right) + \tilde{\Omega}_{n'c}^\dagger \tilde{\Omega}_{nc}^\dagger + \tilde{\Omega}_{nn}^\dagger \tilde{\Omega}_{n'c}^\dagger \tilde{\Omega}_{nc}^\dagger \quad (55)$$

was employed. Note that, with a result for the product of three Møller operators in hand, the expression for the matrix element of  $\Omega_{n'c}^\dagger \Omega_{nc}^\dagger$  can be obtained from Eq. (53) by replacing  $\mathcal{B}_\mu(p, q)$  by  $\mathcal{A}_\mu^{(0)}(p, q)$  and setting the  $\tau_{nn}$  in this formula to zero for all momenta.

In each of these expressions integrals stemming from taking the t-matrix elements have to be evaluated. Limiting ourselves to the case of sharp-cutoff regularization at  $\Lambda$  in the subsystems, i.e.,

$$g_l(p) := p^l \Theta(\Lambda - p), \quad (56)$$

we can use the relation

$$\int dp' p'^2 \frac{g_0(p') f(p', q)}{p^2 - p'^2 + i\epsilon} = \int_0^\Lambda dp' \frac{p'^2 f(p', q) - p^2 f(p, q)}{p^2 - p'^2} - \left( \frac{i\pi}{2} - \frac{1}{2} \ln \left( \frac{\Lambda + p}{\Lambda - p} \right) \right) g_0(p) p f(p, q). \quad (57)$$

For a derivation see the supplemental material of Ref. [50].

## B. Physical properties of approximation schemes

Now we are in a position to calculate the  $E1$  strength distribution for all these additional combinations of Møller operators. The combinations we are interested in are listed in Table I. In the third, fourth, and fifth columns some desirable properties of the resulting matrix element are listed. A particularly important one is the unitarity of the approach: the physical FSIs are norm-preserving, because there is no “probability flow” into bound states in our problem. That means that any violation of unitarity represents a defect of our approximation scheme. Another relevant aspect is if the FSI operator commutes with the  $nn$  permutation operator  $\mathcal{P}_{nn}$ . The full FSI operator commutes with  $\mathcal{P}_{nn}$ , so that the  $nn$  antisymmetry is not broken by FSI. Also here, any violation of  $nn$  anti-symmetry must result from approximations we have introduced. Additional characteristics are the order of the expression in the t-matrices, as well as whether all different two-body interactions up to that order are taken into account. Note that in the table also some abbreviations for the different combinations of operators are introduced: a bar over the subscript  $n$  means that the operator has been averaged between the two identical neutrons, so as to ensure  $nn$  antisymmetry. The bar over  $\Omega_3^\dagger$  in  $\bar{\Omega}_3^\dagger$  indicates that the two different orderings of the Møller operators  $\Omega_{nc}^\dagger$  and  $\Omega_{n'c}^\dagger$  have been averaged. And in both  $(\Omega_3')^\dagger$  and  $(\bar{\Omega}_3')^\dagger$  the prime indicates that the  $nc$  and  $n'c$  interactions come after the  $nn$  interaction, rather than before it.

Table I. Overview of different FSI schemes specified in terms of the used combinations of Møller operators.

operator	max. order in $t_{ij}G_0$	commutes with $\mathcal{P}_{nn}$	unitary	all two-body interactions included
$\mathbb{1}$	0	✓	✓	✗
$(\Omega^{(\text{fo})})^\dagger$	1	✓	✗	✓
$\Omega_{nn}^\dagger$	1	✓	✓	✗
$\Omega_{nc}^\dagger$	1	✗	✓	✗
$\Omega_{nc}^\dagger := \frac{1}{2}(\Omega_{nc}^\dagger + \Omega_{n'c}^\dagger)$	1	✓	✗	✗
$\Omega_{nn}^\dagger \Omega_{nc}^\dagger$	2	✗	✓	✗
$\Omega_{nn}^\dagger \Omega_{nc}^\dagger$	2	✓	✗	✓
$\Omega_3^\dagger := \Omega_{nn}^\dagger \Omega_{n'c}^\dagger \Omega_{nc}^\dagger$	3	✗	✓	✓
$\bar{\Omega}_3^\dagger := \frac{1}{2}\Omega_{nn}^\dagger (\Omega_{n'c}^\dagger \Omega_{nc}^\dagger + \Omega_{nc}^\dagger \Omega_{n'c}^\dagger)$	3	✓	✗	✓
$(\Omega'_3)^\dagger := \Omega_{n'c}^\dagger \Omega_{nc}^\dagger \Omega_{nn}^\dagger$	3	✗	✓	✓
$(\bar{\Omega}'_3)^\dagger := \frac{1}{2}(\Omega_{n'c}^\dagger \Omega_{nc}^\dagger + \Omega_{nc}^\dagger \Omega_{n'c}^\dagger) \Omega_{nn}^\dagger$	3	✓	✗	✓

The table makes it clear that the different combinations have different advantages. The expression using all t-matrices up to first order, i.e. the expression using  $(\Omega^{(\text{fo})})^\dagger$ , has the advantage that  $nn$  antisymmetry is preserved and all interactions are taken into account. However, it is not necessarily unitary. The combination of all three different Møller operators  $\Omega_3^\dagger$  has the advantages of taking all interactions into account and of being unitary. However, it does not commute with  $\mathcal{P}_{nn}$ . It is possible to produce a commutative variant of this combination called  $\bar{\Omega}_3^\dagger$  at the price of losing guaranteed unitarity. In terms of this selection of “features” it is thereby on a par with  $(\Omega^{(\text{fo})})^\dagger$ . However, on a quantitative level there might be significant differences: It might be that the violation of unitarity of  $\bar{\Omega}_3^\dagger$  is much smaller than in the case of  $(\Omega^{(\text{fo})})^\dagger$ .

Before showing the results, we want to mention that in the calculation of the  $E1$  distributions from the matrix elements sums over final-state quantum numbers are involved. In the case of some terms truncations are necessary. A detailed discussion of these sums and the convergence of the truncation can be found in Appendix D.

### C. Numerical results

The  $E1$  distributions based on  $(\Omega^{(\text{fo})})^\dagger$ ,  $\Omega_3^\dagger$ ,  $\bar{\Omega}_3^\dagger$ ,  $(\Omega'_3)^\dagger$ , and  $(\bar{\Omega}'_3)^\dagger$  are shown in Fig. 4. Numerical uncertainties are indicated by bands, which are very narrow here. They were obtained by comparing the calculations with ones having roughly two thirds as many mesh points and a cutoff of three fourths of the original one. The right panel of Fig. 4 contains the cumulative distributions. Some of the distributions already shown in Fig. 2 are also included for comparison.

A striking feature of Fig. 4 is how much the distribution using  $(\Omega^{(\text{fo})})^\dagger$  (green dashed curve) differs from all the others: it has much more strength than any of them. It violates the non-energy-weighted sum rule by a significant margin, attaining an asymptotic value that is roughly twice as large as it should be. The deviation is not totally surprising, as this FSI operator is only an approximation to a unitary Møller operator.

In contrast, there is no large difference between the distribution using  $\Omega_3^\dagger$  (crimson dot-dashed curve) and the one just having  $nn$  FSI (orange dashed curve). This combination of Møller operators includes the same first-order terms in the multiple-scattering series as  $(\Omega^{(\text{fo})})^\dagger$  but is explicitly unitary. It does preserve the sum rule. Including  $n'c$  and  $nc$  interactions via a product of Møller operators moves the peak of the  $E1$  strength distribution to slightly lower energy and increases the peak height slightly. This observation might show that taking products of increasing numbers of Møller operators forms a convergent approximation to the multiple-scattering series at low energies.

$\bar{\Omega}_3^\dagger$  does not need to be unitary, but it gives a result that is indistinguishable from that of  $\Omega_3^\dagger$ . This implies both that  $\bar{\Omega}_3^\dagger$  is approximately unitary (and indeed, it fulfils the sum rule well) and that the violation of antisymmetry in  $\Omega_3^\dagger$  is small.

We also consider the operator  $(\Omega'_3)^\dagger$ , which differs from  $\Omega_3^\dagger$  only in the position of  $\Omega_{nn}^\dagger$ . In  $\Omega_3^\dagger$  it is the first factor in the product of operators, in  $(\Omega'_3)^\dagger$  it is the last one. We also note that results for  $(\Omega'_3)^\dagger$  and  $(\bar{\Omega}'_3)^\dagger$  agree excellently.



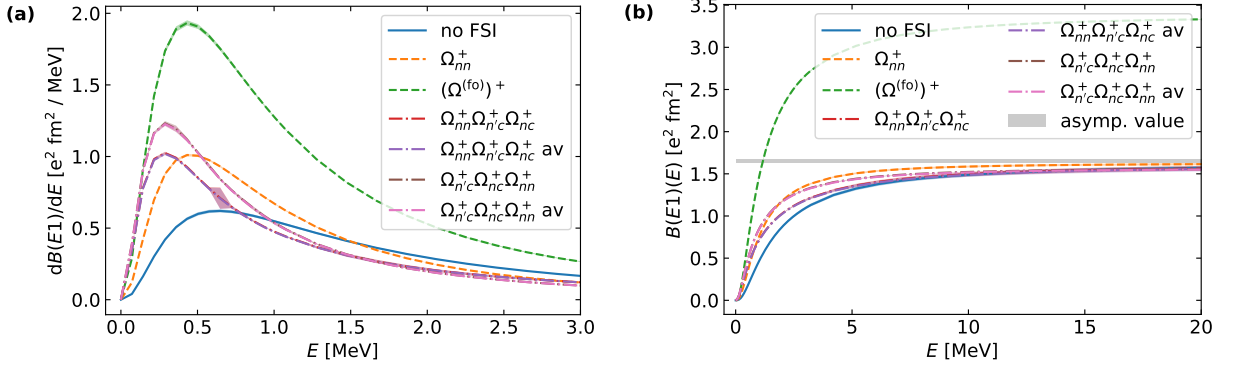


Figure 4. The left panel (a) shows  $E1$  strength distributions of  $^{11}\text{Li}$  with different FSIs including higher-order schemes. The right panel (b) shows the corresponding cumulative  $E1$  strength distributions. The small horizontal band again shows the expected asymptotic value for the cumulative  $E1$  strength distribution, based on  $\langle r_c^2 \rangle$  extracted from  $\mathcal{F}_c(k^2)$ . Note that the results for  $\Omega_{nn}^+ \Omega_{n'c}^+ \Omega_{nc}^+$  and for  $\frac{1}{2} \Omega_{nn}^+ (\Omega_{n'c}^+ \Omega_{nc}^+ + \Omega_{nc}^+ \Omega_{n'c}^+)$  are on top of each other. The same is true for  $\Omega_{n'c}^+ \Omega_{nc}^+ \Omega_{nn}^+$  and  $\frac{1}{2} (\Omega_{n'c}^+ \Omega_{nc}^+ + \Omega_{nc}^+ \Omega_{n'c}^+) \Omega_{nn}^+$ .

Since one is unitary and the other respects  $nn$  antisymmetry this again suggests that violations of these symmetries are small in either approximation scheme. However,  $(\Omega_3^\dagger)^\dagger$  and  $\Omega_3^\dagger$  give somewhat different results. That difference can be taken to be an estimate of the remaining uncertainty in the FSI. This suggests that our approximation to the multiple-scattering series is not fully converged, although the uncertainty due to the approximations used for computing the FSI here is certainly smaller than the uncertainty due to NLO effects.

Any of these combinations of three Møller operators can thus be used for a comparison with experimental data, since they are either exactly, or to a high degree,  $nn$  anti-symmetric and norm preserving. Note that this scheme can not be easily extended to order 4 in the three-body system, since then at least one Møller operator, which we will call  $\Omega_{ij}^\dagger$ , would need to appear two times in the product. Even if there are other Møller operators between the two occurrences, this would also generate an factor of  $t_{ij} G_0^{(ij)} t_{ij} G_0^{(ij)}$  in some term<sup>9</sup> due to the identity terms in the Møller operators between the two occurrences. This would be unphysical, as  $t_{ij}$  fully iterates the  $ij$  interaction and therefore the same t-matrix should not be applied two times directly subsequently with only Green's functions in between. That such a “doubling” is not allowed can also be seen from the expression for the multiple-scattering series in Eq. (38).

#### D. Comparison with other theoretical results and with experimental data

We proceed by comparing our results with experimental data from Ref. [25]. Figure 5 shows our results with different implementations of FSI through combinations of Møller operators. In the left panel the results of our calculations are plotted, in the right panel these theoretical distributions folded with the detector response are shown in comparison with the experimental data<sup>10</sup>. The three results differing in FSIs all have in common that  $nn$  FSI, which turned out to be rather important, is taken into account: the orange dashed line is the result for  $nn$  FSI alone, while the light green and dark green dot-dashed curves are two different orderings of the three possible Møller operators for this system. The difference between the light and dark green curves can thus be taken as an estimate of the uncertainty in our approach. Bands indicating the uncertainties due to truncating the EFT at leading order

<sup>9</sup> The full factor written more formally reads

$$\int dp dq p^2 q^2 \left( |p, q\rangle_k \langle p, q| \otimes \mathbb{1}^{(\text{orbital})} \otimes \mathbb{1}^{(\text{spin})} \right) t_{ij}(E_p) G_0^{(ij)}(E_p) \\ \times \int dq' dp' q'^2 p'^2 \left( |p', q'\rangle_k \langle p', q'| \otimes \mathbb{1}^{(\text{orbital})} \otimes \mathbb{1}^{(\text{spin})} \right) t_{ij}(E_{p'}) G_0^{(ij)}(E_{p'}).$$

<sup>10</sup> Within the folding the finite energy resolution as well as the finite angular resolution reported in Ref. [25] are taken into account. Moreover note that the extraction of the  $E1$  strength from the differential cross section depends on the virtual photon number (cf. Ref. [52]) and thereby also a dependency on the two-neutron separation energy  $S_{2n}$  enters. Ref. [25] from 2006 used  $S_{2n} = 300$  keV. The current value is approximately 369 keV [19]. Therefore, we reextracted the  $E1$  curve using the current value. This reextraction is mainly relevant in  $E < 1$  MeV region, where it changes the peak height by approximately 10 %.

are also shown. We estimated those uncertainties using

$$\Delta\left(\frac{dB(E1)}{dE}\right) = \frac{dB(E1)}{dE} \sqrt{\frac{E}{E^*({}^9\text{Li})}}, \quad (58)$$

whereby  $E^*({}^9\text{Li}) = 2.7$  MeV is the excitation energy of the  ${}^9\text{Li}$  core, which is the lowest scale of omitted physics. The figure clearly shows that, in this leading-order calculation, the EFT uncertainties are larger than the uncertainties due to the treatment of FSI.

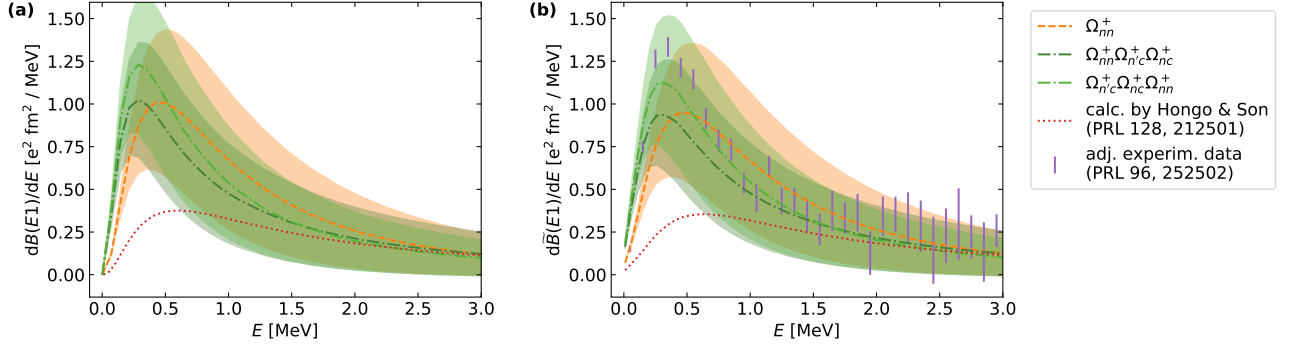


Figure 5. The left panel (a) shows our results for the  $E1$  strength distribution in comparison with the universal curve by Hongo and Son [51]. The right panel (b) shows our results and the result of Hongo and Son folded with the detector resolution in comparison with the experimental data from Nakamura et al. [25] (adjusted to the current  $S_{2n}$  value). The uncertainty bands show the estimated uncertainties of the leading-order EFT results. The uncertainty stemming from approximations of the multiple-scattering series by products of Møller operators can be estimated by comparing the curve using  $\Omega_{nn}^\dagger \Omega_{n'c}^\dagger \Omega_{nc}^\dagger$  with the one using  $\Omega_{n'c}^\dagger \Omega_{nc}^\dagger \Omega_{nn}^\dagger$ .

The prediction of Hongo and Son [51] agrees well with experimental data and our results at higher energies, but has far too little strength at low energies. The doubtful applicability of it to this halo nucleus thereby manifests itself in a low-energy discrepancy from experimental data.

Our different distributions, which all take  $nn$  FSI into account, show qualitative agreement with the experimental values. In the case of the height and width of the low-energy peak there are some discrepancies, which depend also on the concrete FSI approximation scheme. That using solely  $nn$  FSI can lead to good agreement<sup>11</sup> with experimental data can be also seen in Refs. [25, 27].

We conclude that our leading-order calculation of the  $E1$  strength distribution of  ${}^{11}\text{Li}$  agrees reasonably well with experimental data. The FSI approximation technique based on products of Møller operators has proven to be useful, in particular because it provides insight into the role of different FSIs.

## V. CONCLUSION

In this work we calculated the  $E1$  strength distribution of the two-neutron halo nucleus  ${}^{11}\text{Li}$  using a three-body description in Halo effective field theory (EFT) at leading order. We investigated the role of the final-state interactions (FSI) and found that they influence the shape of the distribution significantly. The results show that  $nn$  FSI is the most important single FSI. We also investigated approximations to the full multiple-scattering series that determines the FSI. Including all possible FSIs via a first-order treatment of their t-matrices leads to large unitarity violations, which become manifest in large violations of the non-energy-weighted sum rule. Therefore, we propose a unitary approximation scheme based on products of Møller scattering operators. We were able to verify the expected compliance with the sum rule. In computations up to third order in the t-matrix, the dominance of  $nn$  FSI was confirmed.

We have provided expressions for the  $E1$  distribution with FSI included that are suitable for application to other Borromean  $2n$  halos. In future studies these could be computed in this framework and compared with experimental

<sup>11</sup> However, note that the model of  ${}^{11}\text{Li}$  from Ref. [26] employed along with others in Ref. [27] yields an  $S_{2n}$  of 200 keV in contrast to the current experimental value of 369 keV.

data. Moreover, the convergence pattern of the FSI approximations would be an interesting aspect for further studies. These patterns should also be compared to exact calculations of the three-body scattering state like in Ref. [28] and alternative approaches including full FSI effects such as the Lorentz integral transform method [53].

We also assessed the uncertainty of our calculation. This comes, as explained in the introduction, from: 1) the fact that EFT effects beyond leading order are not included, 2) the treatment of the final state via two-body Møller operators, and 3) basis truncations. The EFT error is, according to the power counting, about 30 % at the  $E1$  peak. We assess the FSI error in this region as about 40 %. The FSI error is much smaller to the right of the peak, and there the EFT error dominates. Errors from truncations are generally smaller than both, and are assessed to be smaller than 5 %. The uncertainties can be reduced in future calculations by going to next-to-leading order in the EFT expansion and by switching from a perturbative calculation of the final state to a full computation of the three-body ( $^9\text{Li}$ -n-n) continuum.

The comparison of the results with experimental data showed good agreement, given that we carried out the calculation only to leading order in Halo EFT. At next-to-leading order (NLO) the impact of low-energy  $p$ -wave resonances in  $^{10}\text{Li}$  will appear as perturbative corrections to both the initial-state bound  $^{11}\text{Li}$  wave function and the FSI. The  $nn$  and  $nc$  effective ranges are also both an NLO effect.

This control over final-state interactions allows us to investigate the impact of different assumptions about the  $^9\text{Li}$ - $nn$  dynamics on the  $E1$  strength distribution. We showed that a description taking all spins into account and using both  $s$ -wave  $nc$  interaction channels ( $s_c - 1/2$  and  $s_c + 1/2$ ) at the same strength yields a good leading-order description of the  $E1$  strength. Conveniently, such a calculation is equivalent to a calculation with only neutron spins included and therefore can be recast as a calculation with a spinless core. We also provided the formalism for a calculation in which only the ( $s_c + 1/2$ ) channel has the low-energy enhancement that leads to the  $^{10}\text{Li}$  virtual state. Such a calculation significantly underpredicts the data. Finally, we compared to the EFT calculation of Hongo and Son [51], which is based on different assumptions about the underlying scales of the  $nnc$  system. In particular, it assumes that the neutron- $^9\text{Li}$  interaction is subleading. The corresponding prediction disagrees with data in the range from  $E = 0$ –1 MeV by a factor of three to four. Since all calculations are adjusted to have the same  $S_{2n}$  of  $^{11}\text{Li}$ , the differences in the  $E1$  distribution genuinely reflect the different assumptions about the  $nc$  subsystem dynamics.

## ACKNOWLEDGMENTS

We thank T. Nakamura for providing the  $E1$  strength data of Ref. [25] and T. Aumann for useful discussions. M.G. and H.W.H. acknowledge support by Deutsche Forschungsgemeinschaft (DFG, German Research Foundation) - Project-ID 279384907 - SFB 1245. H.W.H. has been supported by the German Federal Ministry of Education and Research (BMBF) (Grant No. 05P21RDFNB). B.A. acknowledges support by the Neutrino Theory Network Program (Grant No. DE-AC02-07CH11359). D.R.P. was supported by the US Department of Energy, contract DE-FG02-93ER40756. This work was partially supported through GAUSTEQ (Germany and U.S. Nuclear Theory Exchange Program for QCD Studies of Hadrons and Nuclei) under contract number DE-SC0006758.

## Appendix A: Mapping the calculation with two $nc$ interaction channels onto the spinless calculation

In this section we consider  $2n$  halos where the core as well as the whole halo have spin  $s_c$ . We show that a leading-order description of these systems using two  $nc$  interaction channels ( $s_c - 1/2$  and  $s_c + 1/2$ ) is equivalent to a description with only the neutron spins taken into account and thereby having necessarily only one  $nc$  interaction channel.

*Definitions:* The spin states describing such a system seen from the core as spectator or a neutron as spectator are given by

$$\left| \xi_c^{(\sigma; s_c, M)} \right\rangle_c = \left| \left( \frac{1}{2}, \frac{1}{2} \right) \sigma, s_c; s_c, M \right\rangle_c \quad \sigma \in \{0, 1\}, \quad (\text{A1})$$

$$\left| \xi_n^{(\tau; s_c, M)} \right\rangle_n = \left| \left( \frac{1}{2}, s_c \right) s_c + \tau \frac{1}{2}, \frac{1}{2}; s_c, M \right\rangle_n \quad \tau \in \{-1, +1\}. \quad (\text{A2})$$

The corresponding projection operators are

$$P_c^{(\sigma)} = \sum_M \left| \xi_c^{(\sigma; s_c, M)} \right\rangle_c \left\langle \xi_c^{(\sigma; s_c, M)} \right|, \quad (\text{A3})$$

$$P_n^{(\tau)} = \sum_M \left| \xi_n^{(\tau; s_c, M)} \right\rangle_n \left\langle \xi_n^{(\tau; s_c, M)} \right|. \quad (\text{A4})$$

*Statement:* Having these definitions at hand we can now state that the mapping can be made if the Hamilton operator has the structure

$$H_0 = H_0^{(\text{spatial})} \otimes \mathbb{1}^{(\text{spin})} = H_0^{(\text{spatial})} \otimes (P_c^{(0)} + P_c^{(1)}), \quad (\text{A5})$$

$$V_{nn} = V_{nn}^{(\text{spatial})} \otimes P_c^{(0)}, \quad (\text{A6})$$

$$V_{nc} + V_{n'c} = (V_{nc}^{(\text{spatial})} + V_{n'c}^{(\text{spatial})}) \otimes (P_n^{(-)} + P_n^{(+)}) \quad (\text{A7})$$

and

$$P_c^{(0)} + P_c^{(1)} = P_n^{(-)} + P_n^{(+)} \quad (\text{A8})$$

holds. Equation (A7) means that the spatial/momentum-space part of the  $nc$  interaction has to be the same in  $s_c - 1/2$  and  $s_c + 1/2$ .

More specifically, in this case the Schrödinger equation can be decoupled into one in the  $P_c^{(0)}$ -space and one in the  $P_c^{(1)}$ -space<sup>12</sup>:

$$H = H^{(0)} + H^{(1)} = H^{(\text{spatial}; 0)} \otimes P_c^{(0)} + H^{(\text{spatial}; 1)} \otimes P_c^{(1)} \quad (\text{A9})$$

While the  $P_c^{(1)}$ -space Schrödinger equation misses an  $nn$  interaction, the  $P_c^{(0)}$ -space one is equivalent to a calculation with  $s_c = 0$ . This equivalent equation has the Hamilton operator

$$H^{(0)} = H^{(\text{spatial}; 0)} \otimes P_c^{(0)}, \quad (\text{A10})$$

$$H^{(\text{spatial}; 0)} = H_0^{(\text{spatial})} + V_{nc}^{(\text{spatial})} + V_{n'c}^{(\text{spatial})} + V_{nn}^{(\text{spatial})}. \quad (\text{A11})$$

*Sketch of the proof:* The relation for the projection operators given in Eq. (A8) can be verified by inserting

$$\left| \xi_c^{(\sigma; s_c, M)} \right\rangle = \sqrt{2\sigma + 1} \sqrt{2s_c} \begin{Bmatrix} 1/2 & s_c & s_c - 1/2 \\ s_c & 1/2 & \sigma \end{Bmatrix} \left| \xi_n^{(-; s_c, M)} \right\rangle + \sqrt{2\sigma + 1} \sqrt{2s_c + 2} \begin{Bmatrix} 1/2 & s_c & s_c + 1/2 \\ s_c & 1/2 & \sigma \end{Bmatrix} \left| \xi_n^{(+; s_c, M)} \right\rangle \quad (\text{A12})$$

---

<sup>12</sup> This is because  $V_{nc} + V_{n'c} = (V_{nc}^{(\text{spatial})} + V_{n'c}^{(\text{spatial})}) \otimes (P_c^{(0)} + P_c^{(1)})$  holds then.

into  $P_c^{(0)} + P_c^{(1)}$  and using the ortho-normality relations for the Wigner-6j symbols, as they can be found in Ref. [54]. The other pillar of the proof is to show that in a leading-order calculation with  $s_c = 0$  the Hamilton operator has indeed the form

$$H = H^{(\text{spatial})} \otimes P_c^{(0)}, \quad (\text{A13})$$

$$H^{(\text{spatial})} = H_0^{(\text{spatial})} + V_{nc}^{(\text{spatial})} + V_{n'c}^{(\text{spatial})} + V_{nn}^{(\text{spatial})}. \quad (\text{A14})$$

This can be shown by introducing the spin states  $|\xi_c\rangle_c$  for the  $nn$  interaction channel and  $|\xi_n\rangle_n$  for the  $nc$  interaction channel. As the core has here spin zero and the overall spin is zero, the only allowed  $nn$  spin configuration is zero. Thereby the two states are equal up to a sign and the Hamilton operator for  $s_c = 0$  takes indeed this form.

### Appendix B: Explicit relations for $\mathcal{A}^{(1)}$

In the following we give equations suitable for evaluating  $\mathcal{A}^{(1)}$ , which is defined in Eq. (43):

$$\begin{aligned} \mathcal{A}_{l,\bar{\lambda};\mu;\bar{s},M}^{(1)}(p,q) &= -\sqrt{2\bar{l}+1}\sqrt{2\bar{\lambda}+1} \begin{pmatrix} \bar{\lambda} & 1 & \bar{l} \\ 0 & 0 & 0 \end{pmatrix} \sqrt{\pi} \left( p\bar{f}_{\bar{\lambda}}(p,q) - \frac{1}{2}q\bar{f}_{\bar{l}}(p,q) \right) \\ &\times \left\langle \left( \bar{s}, \frac{3}{2} \right) \frac{3}{2}, M \left| P_{\xi_n} \right| \xi_c^{(M)} \right\rangle_c, \end{aligned} \quad (\text{B1})$$

whereby the round brackets with six arguments denote a Wigner-3j symbol. Equations for  $\bar{f}$  and its ingredients are given below:

$$\begin{aligned} \bar{f}(p,q,x := \cos(\theta_{\mathbf{p},\mathbf{q}})) &:= \frac{1}{\kappa_{cnq}(p,q,x)} \int d\tilde{p}' \tilde{p}'^2 g_0(\kappa_{cnp}(p,q,x)) \tau_{nc}(\kappa_{cnp}(p,q,x)) g_0(\tilde{p}') G_0^{(nc)}(\tilde{p}'; E_{\kappa_{cnp}(p,q,x)}) \\ &\times \sqrt{\pi} \left( -\tilde{p}' \tilde{f}_1(\tilde{p}', \tilde{q}') - \frac{A}{A+1} \tilde{q}' \tilde{f}_0(\tilde{p}', \tilde{q}') \right) \Big|_{\tilde{q}' = \kappa_{cnq}(p,q,x)}, \end{aligned} \quad (\text{B2})$$

$$\tilde{f}(\tilde{p}', \tilde{q}', \tilde{x}' := \cos(\theta_{\tilde{\mathbf{p}}', \tilde{\mathbf{q}}'})) := \frac{f(\kappa_{ncp}(\tilde{p}', \tilde{q}', \tilde{x}'), \kappa_{ncq}(\tilde{p}', \tilde{q}', \tilde{x}'))}{\kappa_{ncq}(\tilde{p}', \tilde{q}', \tilde{x}')}, \quad (\text{B3})$$

$$f(p,q) = i\sqrt{\frac{1}{4\pi}} eZ_c \frac{2}{A+2} (\partial_{\tilde{q}} \Psi_c(p, \tilde{q})) \Big|_{\tilde{q}=q}, \quad (\text{B4})$$

whereby the functions  $\kappa_{ijk}$  ( $i, j \in \{n, c\}$  and  $k \in \{p, q\}$ ) are defined in Ref. [39]. Furthermore, we used the following generic definition of a function  $f_i(p, q)$  via

$$f_i(p, q) := \int dx P_i(x) f(p, q, x). \quad (\text{B5})$$

The  $i$ -th Legendre polynomial is denoted by  $P_i$ .

In order to obtain these expressions inter alia the following relations and techniques were employed:

- relation for expressing  $Y_{l,m}(\mathbf{a} + \mathbf{b})$  using  $Y_{l,m}(\mathbf{a})$  and  $Y_{l,m}(\mathbf{b})$  (see, e.g., Ref. [55]),
- relations for recoupling the Jacobi momenta (see, e.g., Ref. [39]),
- expansion of functions in terms of Legendre polynomials and expressing Legendre polynomials in terms of  $\mathcal{Y}_{l,l}^{0,0}$  (see, e.g., Ref. [55]),
- relation for the integral of three spherical harmonics (see, e.g., Ref. [54]).

### Appendix C: Explicit relations for $\mathcal{A}^{(2)}$

We give an expression for  $\mathcal{A}^{(2)}$ , which is defined in Eq. (44):

$$\begin{aligned} \mathcal{A}_{l,\bar{\lambda};\mu;\bar{s},M}^{(2)}(p,q) &= (-1)^{\bar{l}} \sqrt{\pi} \sqrt{2\bar{\lambda}+1} \sqrt{2\bar{l}+1} \begin{pmatrix} \bar{\lambda} & 1 & \bar{l} \\ 0 & 0 & 0 \end{pmatrix} \left( p\bar{f}_{\bar{\lambda}}^{(2)}(p,q) - \frac{1}{2}q\bar{f}_{\bar{l}}^{(2)}(p,q) \right) \\ &\times \left\langle \left( \bar{s}, \frac{3}{2} \right) \frac{3}{2}, M \left| \mathcal{P}_{nn}^{(\text{spin})} P_{\xi_n} \mathcal{P}_{nn}^{(\text{spin})} \right| \xi_c^{(M)} \right\rangle_c, \end{aligned} \quad (\text{C1})$$

Also here Eq. (B5) applies. The function  $\bar{f}^{(2)}$  is given by

$$\begin{aligned} \bar{f}^{(2)}(p, q, x := \cos \theta_{\mathbf{p}, \mathbf{q}}) &:= \frac{2\pi}{\kappa_{cnq}(p, q, x)} \int d\tilde{p}' \tilde{p}'^2 \tilde{\tau}_{nc}(\kappa_{cnp}(p, q, x)) g_0(\tilde{p}') G_0^{(nc)}(\tilde{p}'; E_{\kappa_{cnp}(p, q, x)}) \\ &\times \left( \tilde{p}' \bar{f}_1^{(2)}(\tilde{p}', \kappa_{cnq}(p, q, x)) - \frac{\kappa_{cnq}(p, q, x)}{A+1} \bar{f}_0^{(2)}(\tilde{p}', \kappa_{cnq}(p, q, x)) \right), \end{aligned} \quad (C2)$$

whereby the short-hand notation  $\tilde{\tau}_{nc}(p) := g_0(p) \tau_{nc}(p)$  is used. Furthermore the definition

$$\begin{aligned} \bar{f}^{(2)}(p, q, x := \cos \theta_{\mathbf{p}, \mathbf{q}}) &:= \tilde{\tau}_{nc}(\kappa'_{nnp}(p, q, x)) \int d\tilde{p}'' \tilde{p}''^2 g_0(\tilde{p}'') G_0^{(nc)}(\tilde{p}'', E_{\kappa'_{nnp}(p, q, x)}) \\ &\times \frac{\sqrt{\pi}}{\kappa'_{nnq}(p, q, x)} \left( -\tilde{p}'' \tilde{f}_1(\tilde{p}'', \kappa'_{nnq}(p, q, x)) - \frac{A}{A+1} \kappa'_{nnq}(p, q, x) \tilde{f}_0(\tilde{p}'', \kappa'_{nnq}(p, q, x)) \right) \end{aligned} \quad (C3)$$

holds.

Also for obtaining these expressions the relations and techniques listed in Appendix B were employed.

#### Appendix D: Sums over the quantum numbers of the final state and their convergence

In this appendix we briefly discuss the handling of the partial waves of the final states. Eqs. (50), (52) and (53) show that only those terms directly proportional to  $\mathcal{A}_{l, \bar{\lambda}; \mu; \bar{s}, M}^{(1)}(p, q)$  or  $\mathcal{A}_{l, \bar{\lambda}; \mu; \bar{s}, M}^{(2)}(p, q)$  are non-zero for multiple combinations of final-state quantum numbers  $\bar{l}, \bar{\lambda}$ . In contrast to that, other terms are only non-zero for  $\bar{l} = 0$  together with  $\bar{\lambda} = 1$ . The expressions for  $\mathcal{A}_{l, \bar{\lambda}; \mu; \bar{s}, M}^{(1)}(p, q)$  and  $\mathcal{A}_{l, \bar{\lambda}; \mu; \bar{s}, M}^{(2)}(p, q)$  in Appendices B and C show that these are already non-vanishing if  $\bar{\lambda} - 1 \leq \bar{l} \leq \bar{\lambda} + 1$ . Using this condition restricts the sum over  $\bar{l}$  for a given  $\bar{\lambda}$  to a finite number of terms, while the sum over  $\bar{\lambda}$  stays in principle unrestricted. Therefore we truncate the sum over  $\bar{\lambda}$  at  $\bar{\lambda}_{\max}$  (inclusive). We usually use  $\bar{\lambda}_{\max} = 5$ , because the relative changes between the results based on  $\bar{\lambda}_{\max} = 3$  and those based on  $\bar{\lambda}_{\max} = 5$  are smaller than 5 % measured in terms of the former. (In fact, in the  $E < 3$  MeV region, which we show in most plots, the relative change is below 2.5 %.) In the case of the quantum number  $\mu$  the sum runs from -1 to 1, and we use the fact that the matrix element is independent of  $\mu$  in order to reduce the numerical costs. The spin of the  $nn$  system in the final state can generally be 0 or 1, while in the case of some terms only 0 is possible. Moreover, sometimes cancellations emerge for certain values naturally because of the nature of the equations. E.g., in the case of  $\Omega_3^\dagger$  the partial wave  $s = 1 \wedge l = 0$  has in principle a non-vanishing contribution, as  $\Omega_3^\dagger$  does not commute with  $\mathcal{P}_{nn}$ , while in the case of  $\bar{\Omega}_3^\dagger$  this contribution is vanishing due to the  $nn$  antisymmetry of the operator.

Finally, we present numerical data on the error originating from the truncation in the quantum number  $\bar{\lambda}$  at  $\bar{\lambda}_{\max}$ . Figure 6 shows the quotients of distributions obtained with  $\bar{\lambda}_{\max} = 5$  and  $\bar{\lambda}_{\max} = 3$ .

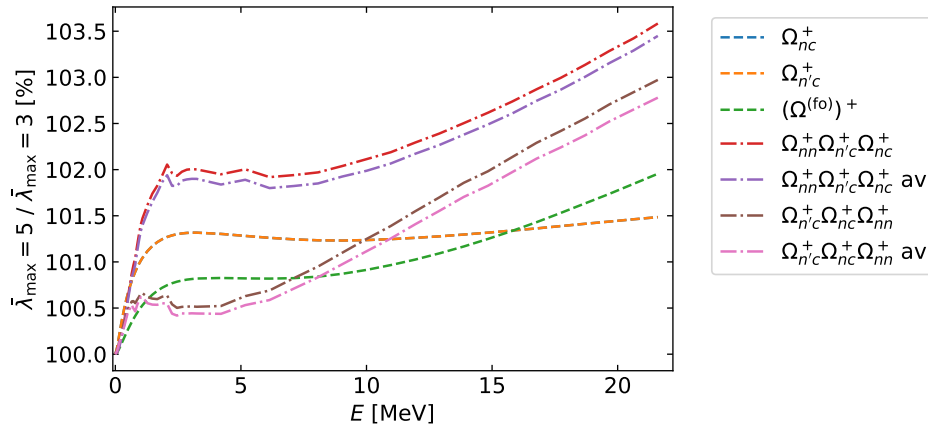


Figure 6. Quotients of  $E1$  strength distributions with  $\bar{\lambda}_{\max} = 5$  and with  $\bar{\lambda}_{\max} = 3$  differing in the FSI treatment.

In the case of the shown distributions the relative changes are smaller than 5 %. Given the significant EFT

uncertainty bands at leading order this is sufficient precision.

- 
- [1] K. Riisager, Phys. Scripta **T152**, 014001 (2013), arXiv:1208.6415 [nucl-ex].
  - [2] H.-W. Hammer, C. Ji, and D. R. Phillips, J. Phys. G **44**, 103002 (2017), arXiv:1702.08605 [nucl-th].
  - [3] I. Tanihata, Eur. Phys. J. Plus **131**, 90 (2016).
  - [4] P. G. Hansen and B. Jonson, Europhys. Lett. **4**, 409 (1987).
  - [5] C. A. Bertulani, H. W. Hammer, and U. Van Kolck, Nucl. Phys. A **712**, 37 (2002), arXiv:nucl-th/0205063.
  - [6] P. F. Bedaque, H. W. Hammer, and U. van Kolck, Phys. Lett. B **569**, 159 (2003), arXiv:nucl-th/0304007.
  - [7] R. Higa, G. Rupak, and A. Vaghani, Eur. Phys. J. A **54**, 89 (2018), arXiv:1612.08959 [nucl-th].
  - [8] P. Premarathna and G. Rupak, Eur. Phys. J. A **56**, 166 (2020), arXiv:1906.04143 [nucl-th].
  - [9] X. Zhang, K. M. Nollett, and D. R. Phillips, J. Phys. G **47**, 054002 (2020), arXiv:1909.07287 [nucl-th].
  - [10] W. Elkhawwy, Z. Yang, H.-W. Hammer, and L. Platter, Phys. Lett. B **821**, 136610 (2021), arXiv:1909.12206 [nucl-th].
  - [11] T. Aumann and T. Nakamura, Physica Scripta **T152**, 014012 (2013).
  - [12] H. W. Hammer and D. R. Phillips, Nucl. Phys. A **865**, 17 (2011), arXiv:1103.1087 [nucl-th].
  - [13] B. Acharya and D. R. Phillips, Nucl. Phys. A **913**, 103 (2013), arXiv:1302.4762 [nucl-th].
  - [14] G. Baur and S. Typel, Prog. Part. Nucl. Phys. **59**, 122 (2007), arXiv:nucl-th/0610082.
  - [15] D. L. Canham and H. W. Hammer, Eur. Phys. J. A **37**, 367 (2008), arXiv:0807.3258 [nucl-th].
  - [16] D. L. Canham and H. W. Hammer, Nucl. Phys. A **836**, 275 (2010), arXiv:0911.3238 [nucl-th].
  - [17] G. Hagen, P. Hagen, H. W. Hammer, and L. Platter, Phys. Rev. Lett. **111**, 132501 (2013), arXiv:1306.3661 [nucl-th].
  - [18] J. Vanasse, Phys. Rev. C **95**, 024318 (2017), arXiv:1609.08552 [nucl-th].
  - [19] M. Wang, W. J. Huang, F. G. Kondev, G. Audi, and S. Naimi, Chin. Phys. C **45**, 030003 (2021).
  - [20] D. R. Tilley, J. H. Kelley, J. L. Godwin, D. J. Millener, J. E. Purcell, C. G. Sheu, and H. R. Weller, Nucl. Phys. A **745**, 155 (2004).
  - [21] W. Nörtershäuser, T. Neff, R. Sanchez, and I. Sick, Phys. Rev. C **84**, 024307 (2011).
  - [22] P. R. Hagen, *Effective Field Theory for Halo Nuclei*, dissertation, University of Bonn (2014).
  - [23] B. Acharya, *Properties of One- and Two-Nucleon Halo Nuclei in Effective Field Theory*, dissertation, Ohio University (2015).
  - [24] B. Acharya and D. Phillips, *Proceedings, 21st International Conference on Few-Body Problems in Physics (FB21): Chicago, IL, USA, May 18-22, 2015*, EPJ Web Conf. **113**, 06013 (2016).
  - [25] T. Nakamura *et al.*, Phys. Rev. Lett. **96**, 252502 (2006).
  - [26] H. Esbensen and G. F. Bertsch, Nucl. Phys. A **542**, 310 (1992).
  - [27] H. Esbensen, K. Hagino, P. Mueller, and H. Sagawa, Phys. Rev. C **76**, 024302 (2007), arXiv:0707.2168 [nucl-th].
  - [28] Y. Kikuchi, T. Myo, K. Kato, and K. Ikeda, Phys. Rev. C **87**, 034606 (2013), arXiv:1302.3004 [nucl-th].
  - [29] S. N. Ershov, J. S. Vaagen, and M. V. Zhukov, Phys. Rev. C **86**, 034331 (2012).
  - [30] M. V. Zhukov, B. V. Danilin, D. V. Fedorov, J. M. Bang, I. J. Thompson, and J. S. Vaagen, Phys. Rept. **231**, 151 (1993).
  - [31] H. Simon *et al.*, Phys. Rev. Lett. **83**, 496 (1999).
  - [32] I. J. Thompson and M. V. Zhukov, Phys. Rev. C **49**, 1904 (1994).
  - [33] A. M. Moro, J. Casal, and M. Gómez-Ramos, Phys. Lett. B **793**, 13 (2019), arXiv:1904.04224 [nucl-th].
  - [34] F. G. Kondev, M. Wang, W. J. Huang, S. Naimi, and G. Audi, Chin. Phys. C **45**, 030001 (2021).
  - [35] M. Zinser *et al.*, Nucl. Phys. A **619**, 151 (1997).
  - [36] H. Böhlen, A. Blazevic, B. Gebauer, W. Von Oertzen, S. Thummerer, R. Kalpakchieva, S. Grimes, and T. Massey, Progress in Particle and Nuclear Physics **42**, 17 (1999), heavy Ion Collisions from Nuclear to Quark Matter.
  - [37] H. B. Jeppesen *et al.*, Phys. Lett. B **642**, 449 (2006).
  - [38] H. Simon *et al.*, Nucl. Phys. A **791**, 267 (2007).
  - [39] M. Göbel, H.-W. Hammer, C. Ji, and D. R. Phillips, Few Body Syst. **60**, 61 (2019), arXiv:1904.07182 [nucl-th].
  - [40] W. J. Huang, M. Wang, F. G. Kondev, G. Audi, and S. Naimi, Chin. Phys. C **45**, 030002 (2021).
  - [41] M. Zinser *et al.*, Phys. Rev. Lett. **75**, 1719 (1995).
  - [42] Y. Aksyutina *et al.*, Phys. Lett. B **666**, 430 (2008).
  - [43] D. E. Gonzalez Trotter *et al.*, Phys. Rev. C **73**, 034001 (2006).
  - [44] R. Sanchez *et al.*, Phys. Rev. Lett. **96**, 033002 (2006), arXiv:physics/0509265.
  - [45] P. A. Zyla *et al.* (Particle Data Group), PTEP **2020**, 083C01 (2020).
  - [46] W. Horiuchi and Y. Suzuki, Phys. Rev. C **76**, 024311 (2007), arXiv:0704.2101 [nucl-th].
  - [47] C. Forssen, V. Efros, and M. Zhukov, Nucl. Phys. A **697**, 639 (2002), arXiv:nucl-th/0108021.
  - [48] J. Taylor, *Scattering Theory: The Quantum Theory of Nonrelativistic Collisions* (Dover Publications, [1972] 2006).
  - [49] C. Möller, Kgl. Danske Videnskab. Selskab, Mat.-fys. Medd. **23(1)**.
  - [50] M. Göbel, T. Aumann, C. A. Bertulani, T. Frederico, H.-W. Hammer, and D. R. Phillips, Phys. Rev. C **104**, 024001 (2021), arXiv:2103.03224 [nucl-th].
  - [51] M. Hongo and D. T. Son, Phys. Rev. Lett. **128**, 212501 (2022), arXiv:2201.09912 [nucl-th].
  - [52] C. A. Bertulani, Theory and Applications of Coulomb Excitation (2009), arXiv:0908.4307 [nucl-th].
  - [53] V. D. Efros, W. Leidemann, G. Orlandini, and N. Barnea, J. Phys. G **34**, R459 (2007), arXiv:0708.2803 [nucl-th].

- [54] D. A. Varshalovich, A. N. Moskalev, and V. K. Khersonskii, *Quantum Theory of Angular Momentum* (World Scientific Singapore, 1989).
- [55] W. Glöckle, *The Quantum Mechanical Few-Body Problem*, Theoretical and Mathematical Physics (Springer Berlin Heidelberg, 1983).